Introduction to the high q^2 analysis of $\Lambda_b^0 \to \Lambda l^+ l^-$

Andrea Treviño Domínguez[†]

This summer, I took the chance to work on an amazing project, with an amazing group. The following is a compilation of what I learnt and did during my internship at CERN in 2021. Some parts I hope they can be useful for new incomers to the area of rare decays and dilepton analyses at LHCb, while others I hope they can be useful for the progress of current LHCb's research.

The quest for New Physics

The Standard Model (SM) of particle physics has been a spectacularly successful theory in providing precise predictions for the properties and interactions of fundamental particles, which have been confirmed by many measurements since its inception in the 1960's [1].

Everything that the Standard Model predicts agrees with experiment, but not every experimental outcome is predicted by the Standard Model. As a fundamental theory, it is generally expected from it to have a say in all fundamental questions, or at least in those we consider fundamental. The theory, however, remains silent on anything that relates to gravity, the apparent dark-matter content of the Universe, or the remarkable difference in the mass scale between the three generations of quarks and leptons.

Therefore, experimental particle physicists are currently invested into discovering new particles and interactions —commonly referred to as 'New Physics'— that could provide an explanation for these observations.

Searches for such new particles are performed in two ways. The first method consists of using ever-increasing centre-of-mass energies in pp collisions, that could lead to the production of new particles (therefore the investment on projects such as the High-Luminosity upgrade, forseen for 2023).

The second method involves performing precise measurements of the properties of known decays of hadrons that are accurately described by the Standard Model, to compare measurement with theory and, hopefully, find some inconsistencies. This is the main approach of the LHCb experiment.

The quest for New Physics at LHCb

At LHCb, rare decays of b- and c-hadrons are of particular interest. As a consequence of quantum-field theory, such decays are allowed to be mediated by particles which physical mass is larger than the available from the mass difference between the final- and initial-state particles. These transient particles are called *virtual*, and include the electroweak gauge bosons, γ, $W^\pm$ and Z^0, and the t quark. However, anomalies with SM predictions could suggest the existence of new particles in these transitions.

When looking for anomalies, the LHCb concentrates in three major battlefields: branching fraction analyses, which are commonly associated to the variable $\mathcal{B}$; branching fraction ratio analyses, associated to the variable R; and angular distribution analyses, which investigate different observables - for instance, the P_5' variable [2].

Anomalies in the first and third kind of analysis could suggest the existence of a new type of particle that would enhance or diminish certain decays, or meddle with the angular distribution of their observables, with respect to the theoretical predictions. Measurements on R, however, compare the likelihoods of semileptonic hadron decays with an electron-positron pair to those with a muon-antimuon pair. Deviations on these from the SM predictions, would indicate a preference in decay for one lepton

[†]CERN Summer Student Program 2021

flavour over the other, suggesting the existence of a new particle that would couple differently to electrons than to muons. This is why analyses of the second type are also referred to as 'lepton-flavour universality tests'.

Cautiously exciting physics

A few months before I commenced my internship at CERN, on the 23rd of March of 2021, some exciting results from the LHCb experiment broke into the headlines of all important newspapers [3][4][5]. The corresponding article presented evidence for the violation of lepton-flavour universality in beauty-quark decays, with a significance of 3.1 standard deviations (see Figure 1). The anomaly was obtained from studies on R_K, involving the $B^+ \to K^+e^+e^-$ and $B^+ \to K^+\mu^+\mu^-$ decays, using proton-proton collision data recorded during the years 2011, 2012 and 2015–2018, in which the centre-of-mass energy of the collisions was 7, 8 and 13 TeV, respectively, and corresponded to an integrated luminosity of 9 fb^{-1} [6].

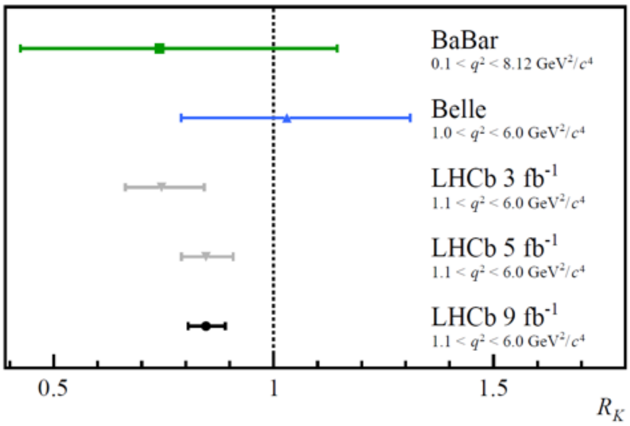

Figure 1. The measured value of R_K by the LHCb, shown as a black point with error bars. This is the most precise measurement to date and is 3.1σ away from the SM prediction, providing evidence for the violation of lepton universality. Results from the BaBar and Belle collaborations are displayed in blue and green, respectively, showing consistency with the Standard Model. Previous measurements from LHCb are also shown with grey color [6].

The results did not come as a surprise for the HEP community: discrepancies on that same analysis had been reported a few years back by LHCb (see data in grey in Figure 1), with lower integrated intensities. The excitement on the measurement lied on its record precision and the $b \to sl^-l^+$ anomaly being present notwithstanding. A lot of other results, reported especially by the LHCb, showed this same interesting tendency.

Figure 2 shows a compilation of some of them, made by Patrick Koppenburg (Nikhef, LHCb collaboration) [7]. One can see the three different experimental variables, $\mathcal{B}, R$ and P_5' that I mentioned before.

For each entry, the theoretical expectation, shown as an orange diamond, is set to zero, and the experimental uncertainty is shifted and scaled accordingly. The graph also shows other measurements such as that from the Muon $g-2$ experiment, at the Brookhaven National Laboratory, and more recent results such as those from the $R_{K^{*+}}$, $R_{K_s^0}$ and $\mathcal{B}(B_s^0 \to \phi\mu^+\mu^-)$.

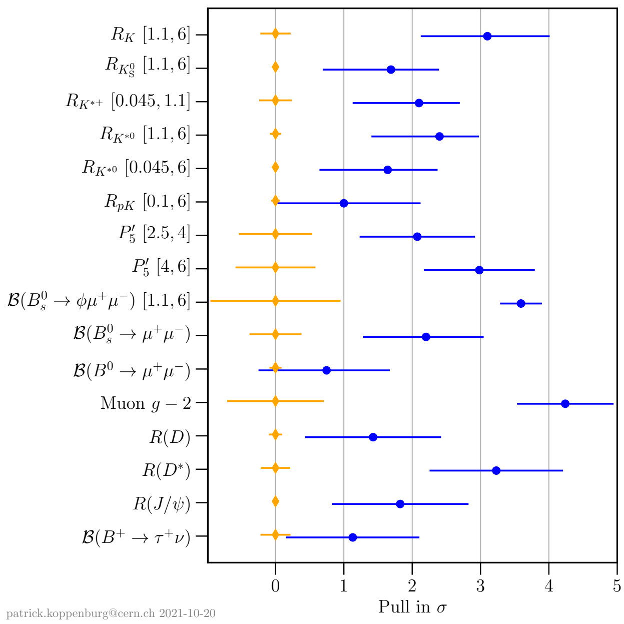

Figure 2. Plot listing some flavour anomalies. Theoretical predictions are set to zero and assigned the orange color. Blue color represents experimental values. For each entry, the type of test and the range of q^2 in which it was performed is shown (when appropriate) - for example, $R_K[1.1, 6]$ refers to the branching fraction analysis in the $q^2 \in [1.1, 6]$ GeV$^2/c^4$ range [7].

Figure 2 seems to be telling us something, and particle physicists wish to know more about it. In the quest for further evidence, a small group at LHCb, informally called the Lb2ll group, is working on the high q^2 analysis of the branching fraction ratio of $\Lambda_b^0 \to \Lambda_b l^+ l^-$ decays, which constitute an example of a FCNC process, highly suppressed at tree level, and only accessible at loop level. It is therefore rare, and a good place to carry additional searches for New Physics.

My role at the CERN Summer Student Program was to work with this team in moving their analysis forward. In practical terms, this meant to study partially-reconstructed backgrounds that may complicate the isolation of our signal and thus worsen the statistics for R_Λ.

In a more **Abstract** manner:

Investigations on the charmonium backgrounds for the $\Lambda_b^0 \to \Lambda l^+ l^-$ decay were examined using the outputs from full Monte-Carlo simulations. The capabilities of the RapidSim software as an alternative light-weight indicator for avenues for further inspection of partially-reconstructed backgrounds were also studied.

Contents

1. Introduction

1.1. Branching fractions and decay widths

A *branching decay* is that which can proceed in two or more different ways (say, n ways). The *branching fraction*, $\mathcal{B}$, is the fraction of particles which decay in a specific way with respect to the total number of decays [8]. If Γ_i refers to the individual decay rate ($i = 1, ..., n$), and Γ_{tot} to the total decay rate, then

$$\Gamma_{\text{tot}} = \sum_i^n \Gamma_i, \qquad [1.1]$$

and

$$\mathcal{B}_i = \frac{\Gamma_i}{\Gamma_{\text{tot}}} = \frac{\tau_{\text{tot}}}{\tau_i} \qquad [1.2]$$

The second equality follows from the fact that a particle's decay rate is equal to the inverse of its (mean) lifetime, τ.

It is common in literature to call Γ the *decay width*. This is because, when considering the quantum-mechanical uncertainty principle,

$$\Delta E \Delta t = \frac{1}{2} \implies \Delta E = \frac{1}{2}\frac{1}{\Delta t},$$

and taking $\Delta t = \tau$,

$$\Delta E = \Gamma/2.$$

The above equation means that the uncertainty on the mass-energy of a particle (its FWHM) gives an estimate on its decay rate. Thus, Γ is called the decay width: a large decay width implies a large uncertainty on the mass energy and short lifetime; a small decay width implies a small uncertainty on the mass energy and a long lifetime.

1.2. Flavour-changing neutral currents in dilepton decays

There are four fundamental forces in the universe: the gravitational force, the electromagnetic force, the strong force and the weak force. The primary role of the weak force is one of decay. It is present, for instance, in the beta decay, or the decay of a neutron (udd) into a proton (uud), an electron and an anti-electron-neutrino[1]. It is therefore related to the lifetime of a particle, and thus, to the branching fraction.

The weak force is mediated by the heavy W^+, W^- and Z^0 bosons. Transitions mediated by the W^+ or W^- boson are known as *charged-current processes* (like beta decay), whereas those mediated by the Z^0 boson are known as *neutral-current processes*.

There are six types (flavours) of quarks: up (u), down (d), charm (c), strange (s), top (t) and (bottom or) beauty (b) . These quarks can change their flavour in a process commonly referred to as *quark-flavour mixing*.

Therefore, a process that transforms one quark into another of different electric charge and different flavour is called a *flavour-changing charged-current* (see Figure 3), while a process that transforms one quark into another of the same electric charge and different flavour is called a *flavour-changing neutral-current* or FCNC (see Figure 4).

[1] Red color indicates quark-flavour mixing, as shown in Figure 3.

Transitions of the first type are allowed at *tree-level* in the SM; however, transitions of the second are only possible at *loop-level* (penguin[2] or box diagrams). The transition

$$q_1 \to q_2\ l^+ l^-, \tag{1.3}$$

is an example of a FCNC process like the one shown in Figure 4. In here q_1 (b) refers to a quark of some flavour, q_2 (s) is another quark of different flavour and lower mass than q_1, and l^+ (μ^+) and l^- (μ^-) conform a lepton-antilepton pair (recall that leptons are either muons, electrons, taus or neutrinos). While leptons are able to exist by themselves, quarks only exist as part of bigger systems called hadrons. Therefore, equation 1.3 can be also written as:

$$H_1 \to H_2\ l^+ l^-, \tag{1.4}$$

where H_1 and H_2 are two different hadrons, composed of either two quarks (mesons), three quarks (baryons) or a higher number of these particles (from here onwards: tetra-quarks, penta-quarks, etc.).

Decays like the one described in equation 1.4 are called *semileptonic*, as their decay products comprise part leptons and part hadrons. Sometimes one can also read/hear expressions like *dielectron* or *dimuon processes* referring to this type of decays, when the lepton particles are electrons or muons respectively.

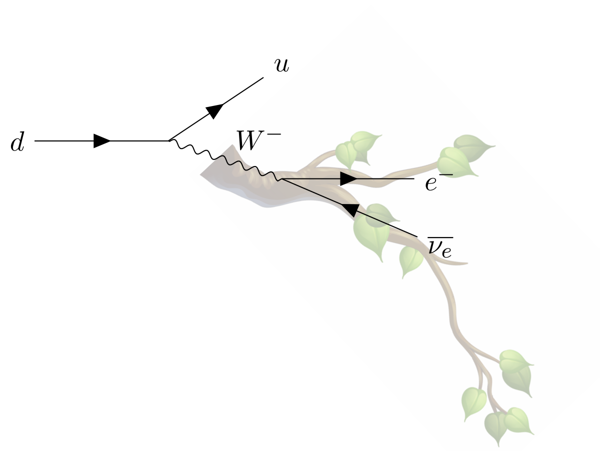

Figure 3. Example of a flavour-changing charged current, possible at **tree-level**. This Feynman diagram describes, for instance, quark-flavour mixing in the (beta) decay $n \to pe^-\overline{\nu_e}$.

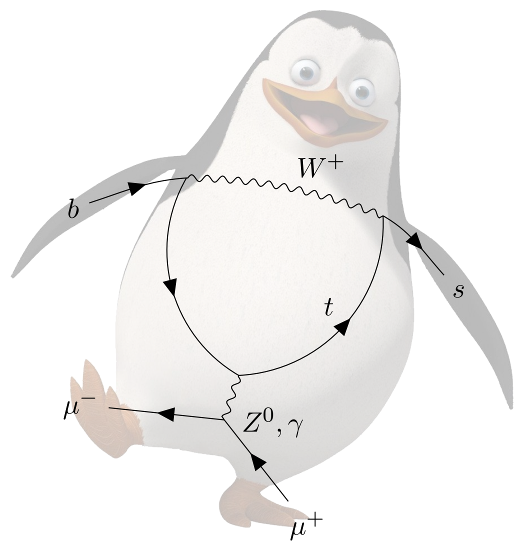

Figure 4. Example of a flavour-changing neutral current, acccesible at **loop-level**. This Feynman diagram describes, for instance, quark-flavour mixing in the (rare) decay $B^+ \to K^+\mu^+\mu-$.

1.3. The Standard Model of rare decays and New Physics

According to Fermi's Golden rule, the decay width or transition rate from an initial state $|i\rangle$ to a final state $|f\rangle$ depends on two factors: the dynamics of the system, encoded in the corresponding element of the transition matrix, $|\langle f|\mathcal{H}|i\rangle|$; and its kinematics or phase space:

$$\Gamma_{i\to f} = \frac{2\pi}{\hbar}|\langle f|\mathcal{H}|i\rangle|^2 \times \langle \text{Lorentz-invariant phase space}\rangle. \tag{1.5}$$

In principle, to calculate the probability amplitude of a decay, $|\langle f|\mathcal{H}|i\rangle|$, we are supposed to add-up the probability amplitudes from all possible Feynman diagrams associated to that decay. In practice, SM calculations go as far as they can get, dealing with leading-order (LO), next-to-leading-order (NLO)

[2]Penguin diagrams are a good remainder of how important it is to perform blind analyses and avoid experimental biases. Most times unconsciously, physicists, as human beings, are tempted to mould reality so as to make it look as they wish.

and next-to-next-leading-order (NNLO) diagrams[3]. The more vertices involved, the more complex the calculation for and the *rarer* the decay is. Tree-like diagrams contain two vertices (coupling constants), while loop diagrams contain at least four.

A FCNC process is only possible at loop-level. Therefore, when someone reads that FCNCs are *suppressed* in the SM, it does not mean that FCNCs are not predicted by the Standard Model, but that they're less likely to occur (compared to, e.g., tree-level processes).

The above (LO/NLO/NNLO approximation)implies that the field operator $\mathcal{H}$ is replaced by an *effective* field operator $\mathcal{H}_{\text{eff}}$, commonly obtained by applying an operator product expansion (OPE) on $\mathcal{H}$. The result is that

$$\mathcal{H}_{\text{eff}} = \sum_i \mathcal{C}_i(\mu, M_W)\mathcal{Q}_i(\mu), \qquad [1.6]$$

where the Hamiltonian is factorised into the Wilson coefficient functions $\mathcal{C}_i$, and the matrix elements of local operators $\mathcal{Q}_i$. This approach is able to achieve a full separation between the long-distance (high-energy) contributions described by C_i, and the short-distance (low-energy) contributions described by $\mathcal{Q}$, both regimes being separated by the renormalisation scale μ [9].

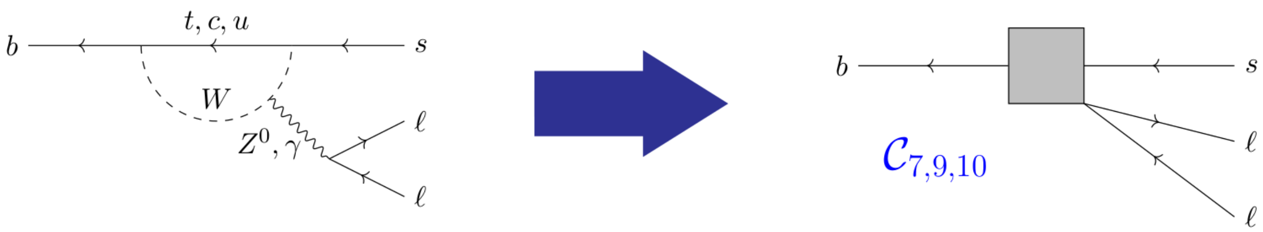

Figure 5. Pictorial representation of the process of integrating out large-mass fields, replacing them with a bunch of effective vertices and associated coupling constants (the Wilson coefficients, $\mathcal{C}_\rangle$. Taken from [10].

As shown in Figure 5, therefore, by using the OPE formalism, one integrates out ('zooms out') fields which masses are larger than the factorization scale μ. These variables are thus removed from the theory as dynamical degrees of freedom, but their existence is still being accounted implicitly, through the Wilson coefficients.

Hence, any precise measurement on the Wilson coefficients associated to a decay which differ from the theoretical predictions, could mean a deviation on their underlying physics: *new physics*.

2. The LHCb detector at the LHC

The Large Hadron Collider (LHC) is the world's highest-energy particle accelerator. It sits 100 metres underground at CERN, the European Organization for Nuclear Research, on the Franco-Swiss border near Geneva, Switzerland. Two beams of protons travelling in opposite directions are accelerated around two separate 27km-long rings to speeds close to the speed of light before being made to collide at four interaction points [12]. In one of those points operates the LHCb experiment.

The LHCb experiment is dedicated to precision measurements of CP violation and rare decays of B hadrons. It is a forward single-arm spectrometer, meaning that the instrument uses a series of subdetectors to detect mainly forward-going particles formed in the proton-proton collisions. This is because most b- and c-hadrons are produced at low pseudo-rapidity (transverse momenta) values [13]. The first subdetector is mounted close to the collision point, with the others following one behind the other over a length of 20 metres.

Closest to the proton-proton interaction region, only 7mm from the beam, is the VErtex LOcator, known as the VELO [14]. It's name reveals its purpose. The VELO measures the distance between

[3] At the moment!

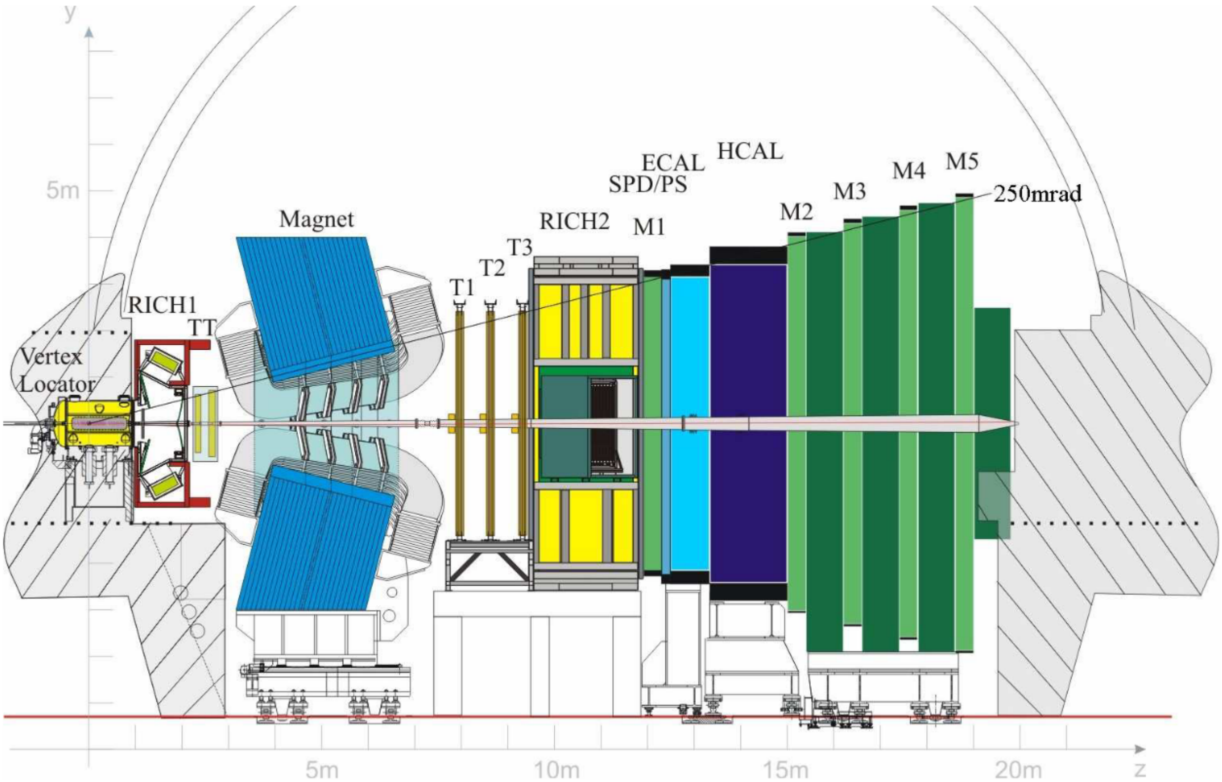

Figure 6. A schematic view of the LHCb detector [11].

the point where protons collide (where b-hadrons are created), called the primary vertex or PV; and the point where the B particles and perhaps other subsequent particles decay (the secondary vertex, SV, and so on) [15]. The B particles are therefore never measured directly[4]. Their presence is inferred from a relatively large impact parameter IP (defined as a minimum distance of the track to the PV, and (relatively) large transverse momentum p_T with respect to the beam axis [16].

After the VELO, there is the first out of the two Ring Imaging CHerenkov (RICH) detectors, which are used for particle identification and attain an excellent separation between K and π mesons in the momentum range from 2 to 100 GeV/c.

After the RICH1 detector, there is the Tracker Turicensis (TT). The TT is part of the Silicon Tracker (ST) system which also includes the Inner Tracker (IT). While the TT is located upstream of the LHCb dipole magnet and covers the full acceptance of the experiment, the IT is found downstream the dipole magnet, and does not cover the full angular range. The IT consists of three stations, called T1, T2 and T3. As one may guess, the complement to an Inner Tracker is an Outer Tracker (OT). Both the VELO, TT, IT and OT detectors allow to keep record of the different particle tracks through the instrument and they all conform the general Tracking System.

Hence, after the TT, there is the spectrometer magnet, a warm dipole magnet which provides an integrated field of 4 Tm. Through the Lorentz force exerted on charged particles, it bends their trajectories according to their momenta. This bending is then recorded in the consequent T1, T2, T3 and OT stations and used to infer the particle's identity.

A second RICH detector, the RICH2 detector, is found after the Outer Tracker; and after this, the Calorimeter and Muon systems comprise the last two sections of the detector.

The Calorimeter system is composed of a Electromagnetic CALorimeter (ECAL) and a Hadron CALorime-

[4] Lifetimes of b-hadrons are extremely short (about 10^{-15}s) and therefore are only allowed to move a few millimeters before decay.

ter (HCAL). It provides the identification of electrons, photons and hadrons as well as the measurement of their energies and positions. The most demanding identification is that of electrons. Therefore, a preshower (PS) and Scintillator Pad Detector (SPD) are used to separate these from the large background of charged pions before entering the ECAL.

Finally, the muon system is placed downstream the calorimeters. It is composed of five stations (M1-M5) of rectangular shape and placed along the beam axis, and is used for muon detection, as the rest of particles (photons, hadrons and electrons) are absorbed by the calorimeters.

3. Backgrounds and data analysis at LHCb

At the primary vertex, one expects all types of particles: the ones we know about for long, the ones we have just recently discovered, like the X(2900) tetraquark, and the ones we still need to discover. There, lie particles of interest such as B mesons and Λ baryons, with very short lifetimes. They soon decay at the secondary vertex, a few milimeters away, into other particles, which can be a combination of these short-lived but also other longer-lived particles such as π and K mesons. Further in time, we're only left with long-standing particles such as neutrons, protons, leptons, pions, kaons and photons.

These stable particles are the ones who manage to traverse the full detector. The (very tricky) job of a particle data analyst is to be able to infer from their tracks, and properties such as their energy, charge and momenta, what happened (what was there) at the primary vertex. This process is called *reconstruction*.

Often, however, scientists are interested not in all the events that happened at the PV, but only in a specific one. In that case, the data is segregated between those reconstructed events that correspond to the branching mode in particular (the signal), and all the other reconstructed events that did not follow the desired decay mode (the backgrounds).

The classification between what is signal and what is background is not an easy task. In fact, this is the main challenge in the job of a particle data analyst (apart from making plots in ROOT). For example, imagine we are interested in decays with the format $B_s^0 \to K^+K^-$. The following decay, $B_d^0 \to K^+K^-$ happens, but instead is reconstructed as $B_s^0 \to K^+K^-$. It has been classified as signal, even though the mother particle was a B_d^0 meson instead of a B_s^0 meson, becoming therefore a background event.

To investigate backgrounds like the one described, and other types of background, data analysts resort to Monte Carlo simulations. The output of these simulations is what is often referred to as *MC samples*. These are generated through a lengthy process. Briefly, the software **Gauss** is used for the event generation (**Pythia**), decay (**EvtGen**) and tracking of particles through the detector layout (**GEANT4**). The software **Boole** mimics the detector response, and this is input onto **Moore** to emulate the L0 trigger. From here on, the simulated data goes through the High Level Trigger system (with the Moore software) and identical reconstruction and stripping processes as that of the data collected by the Data Acquisition (DAQ) system [17]. Figure 7 shows the layout of the whole case.

3.1. Truth-matching and background-category conditions

The advantage of numerical simulations over experiment is that in the proper we know what happened, we know the *truth*. Therefore, in the Monte-Carlo simulation of a decay, there are MC events and true MC events. The process of trying to match an MC event to a true MC event is called *truth-matching*. There are, however, three and not two types of event that we need to pay attention to: the reconstructed MC event, the true MC event and the descriptor event. The latter is the one we input in the descriptor (DEC) file, and is the one we wish to investigate.

In a Monte-Carlo simulation, an event is classified as signal when:

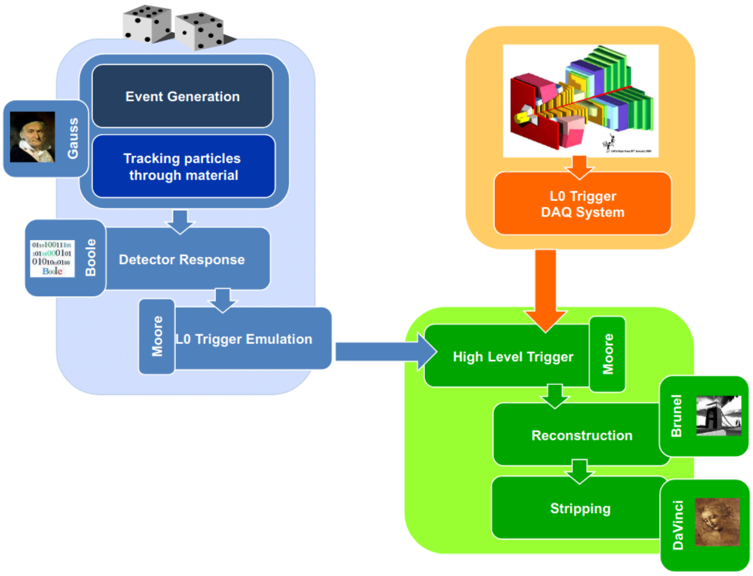

Figure 7. Outline of the LHCb data processing, borrowed from [17]. In blue there is the Monte Carlo sample production, the orange region encapsulates the Data Taking process in an actual experiment, and the Reconstruction and stripping for both the MC and the data collected by the DAQ of the experiment are in green.

1. each final state particle of the reconstructed event has an associated particle in the true MC event with the same particle ID (PID);
2. the true MC particle has the same head, same final-state particles and same topology as the signal decay, but it can differ from it by the presence or absence of intermediate resonances.
3. all intermediate states listed in the descriptor are found in the reconstructed MC decay.
4. all particles in the true MC event have a common mother;
5. there is a one-to-one correspondence between the final-state particles of the reconstructed event and the final-state particles of the true MC event; and
6. the mother particle in the reconstructed MC event has the same PID as the mother particle in the true MC event.

For example, imagine your DEC file holds the following decay [18]:

$$\begin{aligned} B_s^0 &\to D_s^\pm + \pi^\mp \\ &\quad D_s^\pm \to K^+ + K^- + \pi^\pm \end{aligned}$$

A true MC decay has the following form:

$$\begin{aligned} B_s^0 &\to D_s^\pm + \pi^\mp \\ &\quad D_s^\pm \to \phi^0 + \pi^\pm \\ &\qquad \phi^0 \to K^+ + K^-. \end{aligned}$$

Your reconstructed decay is found to be:

$$\begin{aligned} B_s^0 &\to D_s^\pm + \pi^\mp \\ &\quad D_s^\pm \to K^+ + K^- + \pi^\pm \end{aligned}$$

The final-state particles of the reconstructed decay match those from the true MC decay and from the signal. The true MC decay differs from the signal decay by an intermediate state. All intermediate states in the signal decay are found in the MC event. The reconstructed MC decay is a signal event.

However, imagine that your DEC file instead holds the decay

$$\begin{aligned} B_s^0 &\to D_s^\pm + \pi^\mp \\ &\quad D_s^\pm \to \phi^0 + \pi^\pm \\ &\quad\quad \phi^0 \to K^+ + K^-. \end{aligned}$$

Your true MC decay is given by

$$\begin{aligned} B_s^0 &\to D_s^\pm + \pi^\mp \\ &\quad D_s^\pm \to K^+ + K^- + \pi^\pm, \end{aligned}$$

which fully matches the reconstructed MC decay,

$$\begin{aligned} B_s^0 &\to D_s^\pm + \pi^\mp \\ &\quad D_s^\pm \to K^+ + K^- + \pi^\pm. \end{aligned}$$

In this case, the reconstructed MC event won't copy all intermediate states of the signal's decay, and the event is categorised as *quasi-signal*.

Everything that does not fulfill the conditions for a signal or quasi-signal event, is classified as background. There are, however, different types of backgrounds. These can be classified into two main groups: the physics backgrounds, caused by the reconstruction of all or part of an actual physics decay, and technical and combinatoric backgrounds, caused by reconstruction of particles which did not really exist in the event [19]. The proper commonly encompass fully-reconstructed, partially-reconstructed and reflection backgrounds:

- **Partially-reconstructed background**. Independently of the signal descriptor, a reconstructed MC decay, given by

  $$\begin{aligned} B^- &\to D^0 + \pi^- \\ &\quad D^0 \to K^- \pi^+ \end{aligned}$$

  is matched to the true MC decay given by:

  $$\begin{aligned} \Lambda_b &\to \Lambda_c + \pi^- \\ &\quad \Lambda_c \to p K^- \pi^+; \end{aligned}$$

  that is, the truth-matching ignored the p particle of the true MC decay. This is called a partially-reconstructed background: the true MC signal was partially reconstructed by the reconstructed event. A special type of partially-reconstructed background is the **low-mass background**, when the reconstructed particle is found to have a mass systematically below the signal peak [19].

- **Fully reconstructed background**. In this case the topology is correctly and fully reconstructed, but the PID of the parent particle in the reconstructed event does not match the one from the true MC event. The previous example with $B_d^0 \to KK$ decay is an instance of a fully-reconstructed background with same final-state particle but different parent particle. It can be the other way around too, with, say, the B meson from $B^0 \to \pi^+ \overline{D}^0 \pi^-$ taken as the B meson from $B^0 \to K^+ \overline{D}^0 \pi^-$.

- **Reflection background**. This background occurs when a final-state particle is misidentified (for instance, a pion is identified as a kaon). Then, a decay $D^0 \to K^- \pi^+$ is considered the same as $D^0 \to K^- K^+$. Recall that distinction between kaons and pions is done by the RICH detectors.

The technical or combinatoric backgrounds present a wider variety and can be briefly described:

- **Ghost-particle background**. This category includes any reconstructed MC decay in which one or more of the final-state particles have no associated particle in the true MC event. These particles are therefore termed as *ghosts*.
- **Primary-vertex background**. This happens when one or more final-state particles of the reconstructed MC event are said to come from the primary vertex, when this was not the case in the true MC event.
- **Badly-reconstructed-primary-vertex background**. This happens when the primary vertex of the reconstructed MC event is misplaced from that of the true MC event.
- **Pile-up background**. This includes any reconstructed MC event in which one or more final-state particles have been found to come from different primary vertices.
- **$b\bar{b}$ background**. Any background that does not fit any of the previous background categories and which at least one of the final-state particles has a mother with bottom content.
- **$c\bar{c}$ background**. Similar to the above but with charm content.
- **uds background**. Any background that does not fit in any of the previous background categories mentioned.

When a MC sample is produced and we wish to make some plots on the distribution of a variable, for example, Lb_q2, we can investigate the effects that these backgrounds have on our signal by using `Lb_BKGCAT`, by applying *background conditions*. The variable `Lb_BKGCAT` can be set equal to a number, associated to a different type of event. The numbers used in this paper are: 0, for signal; 10, for quasi-signal; 50, for low-mass background; and 60 for ghost-particle background. For example, considering again the variable Lb_q2 from the MC sample associated to the $\Lambda_b \to \Lambda l^+ \, l^-$, we can specify in the `Draw` conditions of our ROOT macro that `Lb_BKGCAT == 0 || Lb_BKGCAT == 10`, meaning: 'Please, plot me a histogram with the distribution of the Lb_q2 associated to the `Lb2LEE` decay that was only either classified as signal or quasi-signal'.

3.2. Bremsstrahlung radiation and photon-multiplicity conditions

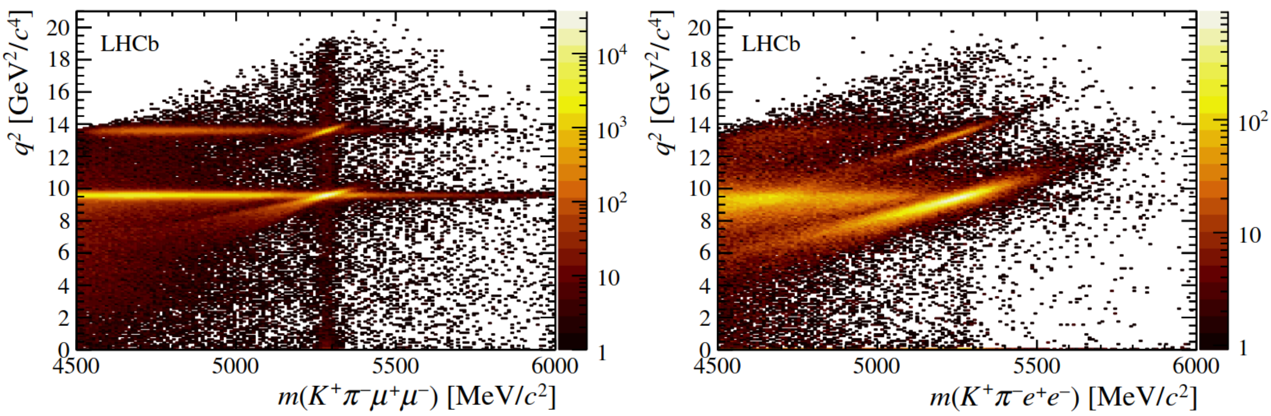

Figure 8. Plot of the dilepton invariant mass squared, q^2 against the B^0 invariant mass for $B^0 \to K^{*0}(\to K^+\pi^-)l^+l^-$, with muons (left) and electrons (right) [20].

At the LHCb detector, dilepton decays with muons have a much better momentum (thus, dilepton invariant mass) resolution than electrons. This is due to energy loss through Bremsstrahlung radiation.

Low-mass charged relativistic particles do not decelerate by ionisation but by radiating Bremsstrahlung photons. The energy loss (energy of the radiated photons) through Bremsstrahlung is inversely proportional to the square of the probe's mass (the lepton's mass in our case). The muon mass is about 200 times greater than that of the electron and, consequently, Bremsstrahlung radiation, if not accounted for, affects greatly the event reconstruction of electron momenta with respect to that of the muon, resulting in a remarkable difference in the sharpness of their signatures in plots like the one shown in Figure 8 (The two graphs correspond to the $B^0 \to K^{*0} l^+ l^-$ decay, but are characteristic of dilepton analyses in general). The procedure of going from *momentum smearing.*

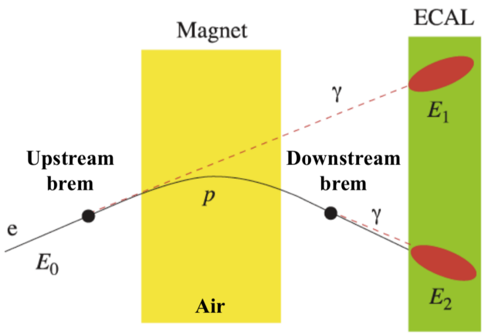

Figure 9. Diagram showing two possible scenarios in Bremsstrahlung (briefly, Brem) radiation. When Brem radiation occurs downstream of the dipole magnet, the momentum of the electron is correctly measured, as the photon energy is deposited in the same calorimeter cell as that of the electron. On the other hand, when Brem radiation occurs upstream the dipole magnet, the photon energy is deposited in a different cell to that of the electron [21].

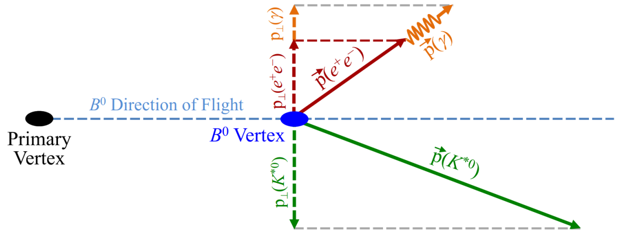

Figure 10. Sketch of the topology of a $B^0 \to K^{*0} e^+ e^-$ decay. The transverse momentum ($p_\perp$) of the Bremsstrahlung photon is calculated as the difference between the transverse momentum of the excited kaon K^{*0} and the transverse momentum of the dielectron system with respect to the flight direction of the B^0 meson [20].

Before reaching the ECAL, electrons are made to pass through a magnetic field which bends their trajectory, as shown in Figure 3.2. The magnetic field area is filled with air and therefore Bremsstrahlung radiation is most likely to happen at the TT region before the dipole magnet or at the PS/SPD subdetector after it. If Bremsstrahlung radiation occurs before entering the magnetic field region (upstream), the electron's trajectory will deviate from that of the emitted photon and each will interact with different cells of the ECAL. On the other hand, if Bremsstrahlung radiation occurs after leaving the magnet (downstream), the emitted photon and electron will reach the same ECAL cell.

The upstream scenario complicates momentum reconstruction, and a dedicated Bremsstrahlung recovery procedure is used, correcting the measured electron momentum by the Bremsstrahlung photon energy. A search is made for photons with transverse energy greater than 75 MeV[5] within a region of the ECAL defined by the extrapolation of the electron track upstream of the magnet. The minimum value for p_T for oppositely-charged electron pairs is constrained to a certain number and a good quality vertex is often required. Bremsstrahlung photons that are not recovered by the reconstruction are assumed to follow the dielectron momentum direction.

Hence, in the momentum reconstruction for each electron, one is presented with two possible scenarios: No Brem recovery (no photon is found to fulfill the above conditions, cannot be matched to the specific electron, and therefore it is assumed to have arrived along with the particle at the ECAL) or Brem recovery (a photon has been found to fulfill all the above conditions and can be associated to the specific electron). When considering the dielectron system, the two cases become three: either no photon, one photon, or two photon recoveries.

In the MC samples of semileptonic decays, the variable `Lb_q2` refers to the square invariant-mass of the reconstructed MC dilepton system, while the variable `Lb_q2_nobrem` refers to the square invariant-mass of the reconstructed MC dilepton system when effects of Bremsstrahlung radiation are not considered -that is, in this variable, the energy and momenta recorded at the detector of the two electrons is not modified with any recovery of some kind. In addition to these two variables, it is possible to play with the *photon-multiplicity conditions.* These are like the background conditions mentioned above

[5] See Figure 10 for clearance on how the transverse momentum of the emitted photon is derived.

(in the sense that they can be applied in the same contexts) but instead allow us to check for all the events that have been assigned a none, one or two Brem-photon recovery. For instance, we could write `L1_BremMultiplicity + L2_BremMultiplicity == 1`, on the distribution of `Lb_q2` to obtain only the `Lb_q2` events for which the photon-multiplicities of the two electrons sums-up to one - i.e., either the electron or the positron were assigned a Brem-photon, but not both.

4. The R_Λ analysis case

4.1. The interest in Λ baryons

A baryon of type Λ is comprised of a ud quark-pair and a third quark of either the second or third generation (s, c or b[6]). The decay of Λ_b^0 (udb) to a Λ^0 (uds) and a muon-antimuon or electron-antiproton pair is $b \to sl^+l^-$ FNCN process (i.e., its Feynman diagram may follow Figure 4). This type of processes are strongly suppressed in the Standard Model, but still less suppressed than other semi-leptonic FCNC transitions such as $c \to ul^+l^-$ or $t \to cl^+l^-$, which makes them interesting for analysis [22].

The $\Lambda_b \to \Lambda(\to p^+\pi^-)l^+l^-$ decay provides a wide variety of angular observables that can be used to disentangle the contributions from individual operators in the $b \to sl^+l^-$ effective Hamiltonian [23]. The Λ_b^0 baryon also has non-zero spin, which opens the door towards improvements in the currently limited understanding of the helicity structure of the underlying Hamiltonian. Its composition can also be seen as consisting of a heavy quark with a light diquark system, which differs from that of B mesons, and may shed light into the understanding of the latter [24]. Additionally, the $\Lambda_b \to \Lambda(\to p^+\pi^-)l^+l^-$ form factors can be calculated to high precision using standard methods in lattice QCD.

One disadvantage of Λ_b baryons may lie in the viewpoint of the experiment, as their production rate is about four times less than that of the B meson [25]. Additionally, the reconstruction efficiency for Λ_b baryons is lower than that of stable particles like p^+, K^+ or π^+, as they need to decay in time for the p^+ and π^- (its decay products) to be detected.

4.2. The interest in the high q^2 region

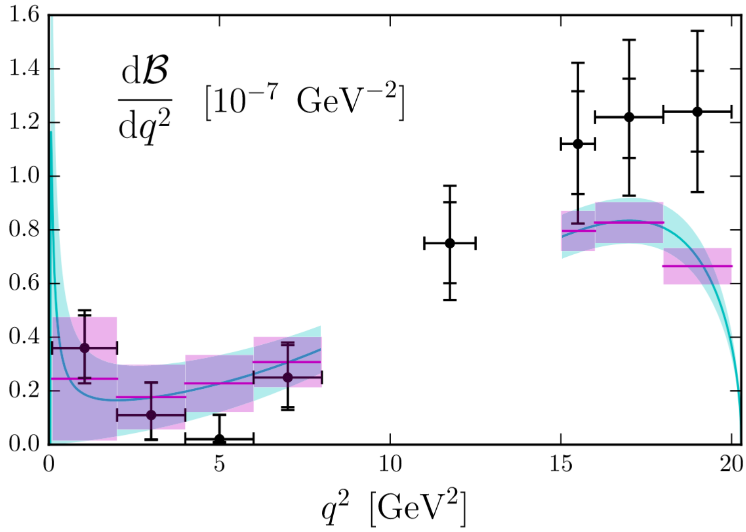

Figure 11. Plot from [26], comparing the $\Lambda_b \to \Lambda\mu^+\mu^-$ differential branching fraction calculated in the Standard Model to the experimental data from LHCb.

In 2016, the current best prediction for the differential branching fraction of $\Lambda_b \to \Lambda(\to p^+\pi^-)\mu^+\mu^-$ decay was published by LHCb [26]. The corresponding experimental result measured at LHCb currently

[6] Not t as they just decay too fast!

exceeds this by 1.6σ in the (high) $15.0 < q^2 < 20\ \mathrm{GeV}^2/c^4$ region, where both experiment and theoretical measurements are more precise (see Figure 11). Even though the discrepancy is not statistically significant, it happens to occur in the opposite direction to what has been observed in other B meson decays, suggesting the need for further work on more precise experimental results in this bin, including those for the branching ratio of the normalization mode $\Lambda_b \to J/\psi\Lambda$.

4.3. The interest in a LFU test

After seeing the overwhelming tendency towards LFU violation of many other dilepton studies, the Lb2Lll group at LHCb was founded to investigate, amongst other things, how carrying out such type of test in the high q^2 region of $\Lambda_b^0 \to \Lambda l^+ l^-$ decays would be like.

As mentioned previously, the associated variable for this type of analysis is R, and its value is obtained from the following formula:

$$R_H[q^2_{\min}, q^2_{\max}] = \frac{\int_{q^2_{\min}}^{q^2_{\max}} dq^2 \frac{d\mathcal{B}(H_1 \to H_2 \mu^+\mu^-)}{dq^2}}{\int_{q^2_{\min}}^{q^2_{\max}} dq^2 \frac{d\mathcal{B}(H_1 \to H_2 e^+e^-)}{dq^2}}, \qquad [4.7]$$

with $q^2 = m^2(l^+l^-)$ and $H = K, K^+, \phi...$[7]. The R_H variable is called the branching fraction ratio, as mentioned previously, and it constitutes a rather clean way of measuring deviations from the SM predictions on the electroweak couplings between electrons and muons.

4.4. The challenges of the $\Lambda_b^0 \to \Lambda l^+ l^-$ analysis

The decay $\Lambda_b^0 \to \Lambda l^+ l^-$, with $l = e, \mu$ is a rare ($b \to s$) flavour-changing neutral current process which proceeds through electroweak loop (penguin and $W^\pm$ box) diagrams. Therefore, it is highly suppressed at tree level and can be used to search for physics beyond the SM.

We are interested on the decays which took the following decay path:

$$\begin{aligned} \Lambda_b^0 &\to \Lambda + l^+ + l^- \\ &\quad\ \Lambda \to p + \pi^- \end{aligned}$$

The statistics on the signal is haunted, firstly, by the *charmonium decays*[8], the $\Lambda_b \to \Lambda(\to p^+\pi^-)J/\psi(\to l^+l^-)$ and the $\Lambda_b \to \Lambda(\to p^+\pi^-)\psi(2S)(\to l^+l^-)$ modes. As indicated previously, the MC sample will not differentiate between these *resonant decays*[9] and the true signal decay. Therefore, it is necessary to separately count with the MC samples of these two. Secondly, Bremsstrahlung radiation worsens the resolution of the invariant mass squared of the dielectron system, and thus complicates any precision measurement on the branching fraction ratio. Thirdly, we have the partially-reconstructed backgrounds of decays involving Λ-baryon excited states, as well as other baryons, such as Ξ.

In addition, the primary decay mode of the Λ_b baryon is $p\pi^-$, but followed by it there are the $n\pi^0$ and $n\gamma$ branching modes. The trouble with these two last ones is that they both consist of neutral particles, which energy resolution at the electromagnetic calorimeter is lower than that of charged particles. The performance of the hadronic calorimeter is even worse, and therefore neutral hadrons such as neutrons won't be reconstructed without further constraints. In a similar manner, neutral particles can be found in the excited-state decays and other baryonic decays.

[7] As can be seen in Equation 4.7, the branching fraction B is found to depend on the square of the invariant mass of the dilepton system; that is, how often Λ_b^0 baryons decay in the mode ($\Lambda_b^0 \to \Lambda^0 l^+ l^-$) we are interested in, depends on the energy of the two electrons. Therefore, it is common in LFU tests, and and so is in this paper, to find references to the variable q^2.

[8] Charmonium as they contain charm! In fact $\psi(2S)$ is just an excited state of J/ψ.

[9] They are so-called because they occur at tree-level and therefore are more commonly seen.

5. Background studies with MC samples

Having the MC samples for the signal decay `Lb2LEE`, and the resonant `Lb2LPsiEE` and `Lb2LJPsEE` decays, the first task was to see how much these override the signal. This is shown in the four plots of Figure 12. In the graph at the top-left corner, one can observe the two peaks, green and blue, corresponding to the `Lb2LJPsEE` and `Lb2LPsiEE` decays, respectively; and the dominance of `Lb2LEE` events over `Lb2LPsiEE` events after $q^2 \sim 15\ \mathrm{GeV}^2/c^4$. In the top-right plot, it is shown the `Lb_q2_nobrem` distribution instead, and the threshold is set to a lower value, $q^2_{\mathrm{nobrem}} \sim 14\ \mathrm{GeV}^2/c^4$. The bottom row displays the same data but zoomed in the horizontal axis. One thing to note is the reduction in the $\psi(2S)$ signal for the q^2_{nobrem} case.

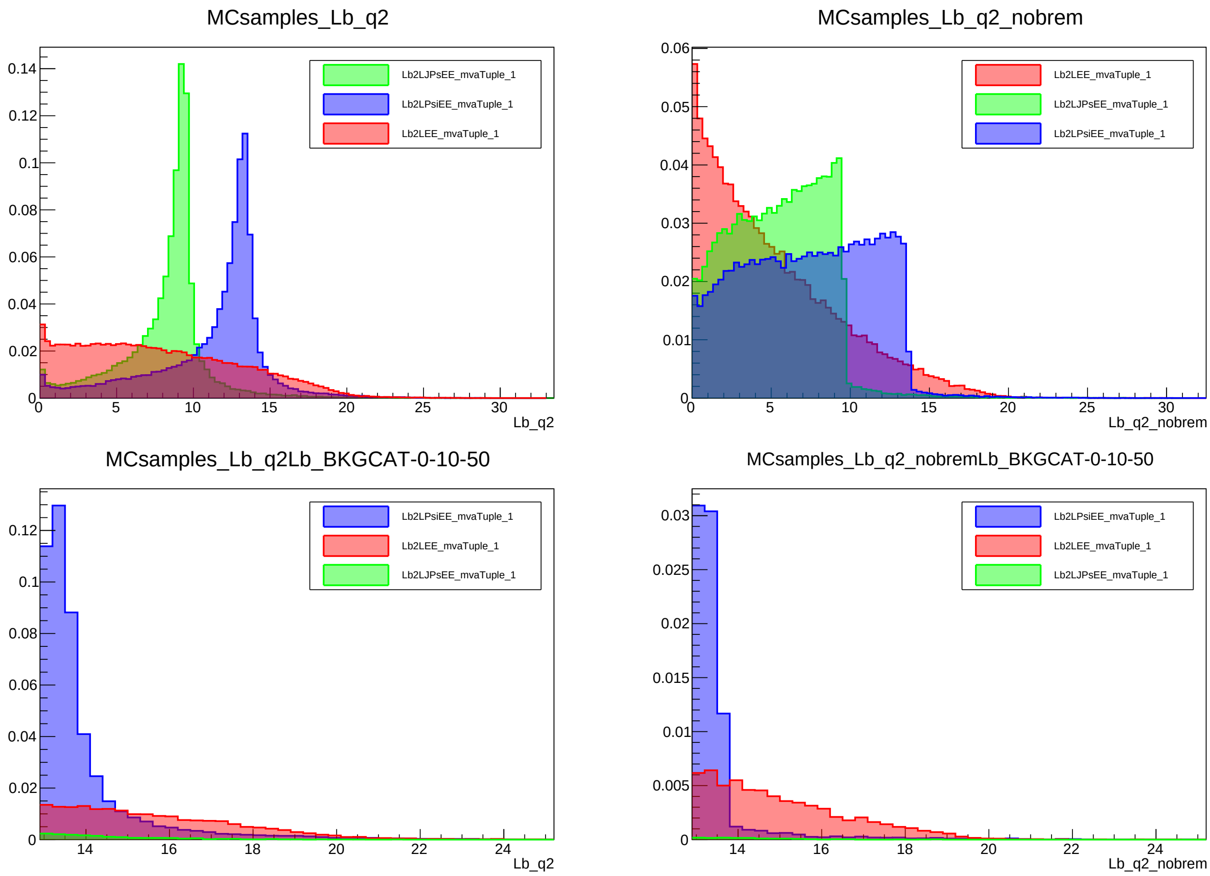

Figure 12. Normalised distributions of `Lb2LJPsEE` (green), `Lb2LPsiEE` (blue) and `Lb2LEE` (red) over region of interest of the dielectron invariance mass, `Lb_q2` (q^2) -left-, and over region of interest of the dielectron invariance mass without adding Bremsstrahlung energy, `Lb_q2_nobrem` -right-. Condition `Lb_BKGCAT=0 || Lb_BKGCAT=10 || Lb_BKGCAT=50` is applied. Mass units are in GeV^2/c^4. Top row goes over the whole q^2 range while the bottom row focusses on the high q^2 region.

Having the possibility to investigate the effects of applying different background conditions on the samples, we do so in Figures 13 and 14 to the distributions of the `Lb_q2` and `Lb_q2_nobrem` variables. The second Figure is the same as the first, but zoomed in the high q^2 region. Next to each color in the legend, the numbers used for the `Lb_BKGCAT` conditions are displayed. For instance, the blue color means a condition `Lb_BKGCAT == 0 || Lb_BKGCAT == 10 || Lb_BKGCAT == 50` was applied on the distribution. For the `Lb2LEE` decay, all various distributions match closely, even when the region is zoomed-in. However, in the other two decays, the green and red are closer together than to the blue and magenta distributions. One can see too the disappearance of the bump at low q^2 (middle row, Figure 13) when the ghost-particle background (`Lb_BKGCAT == 60`) is removed. It seems, from the bottom plots from Figure 14, that low-mass background do not affect the high q^2 regions, as one might expect. However, ghost-particle background are still present in this range, as well as other backgrounds.

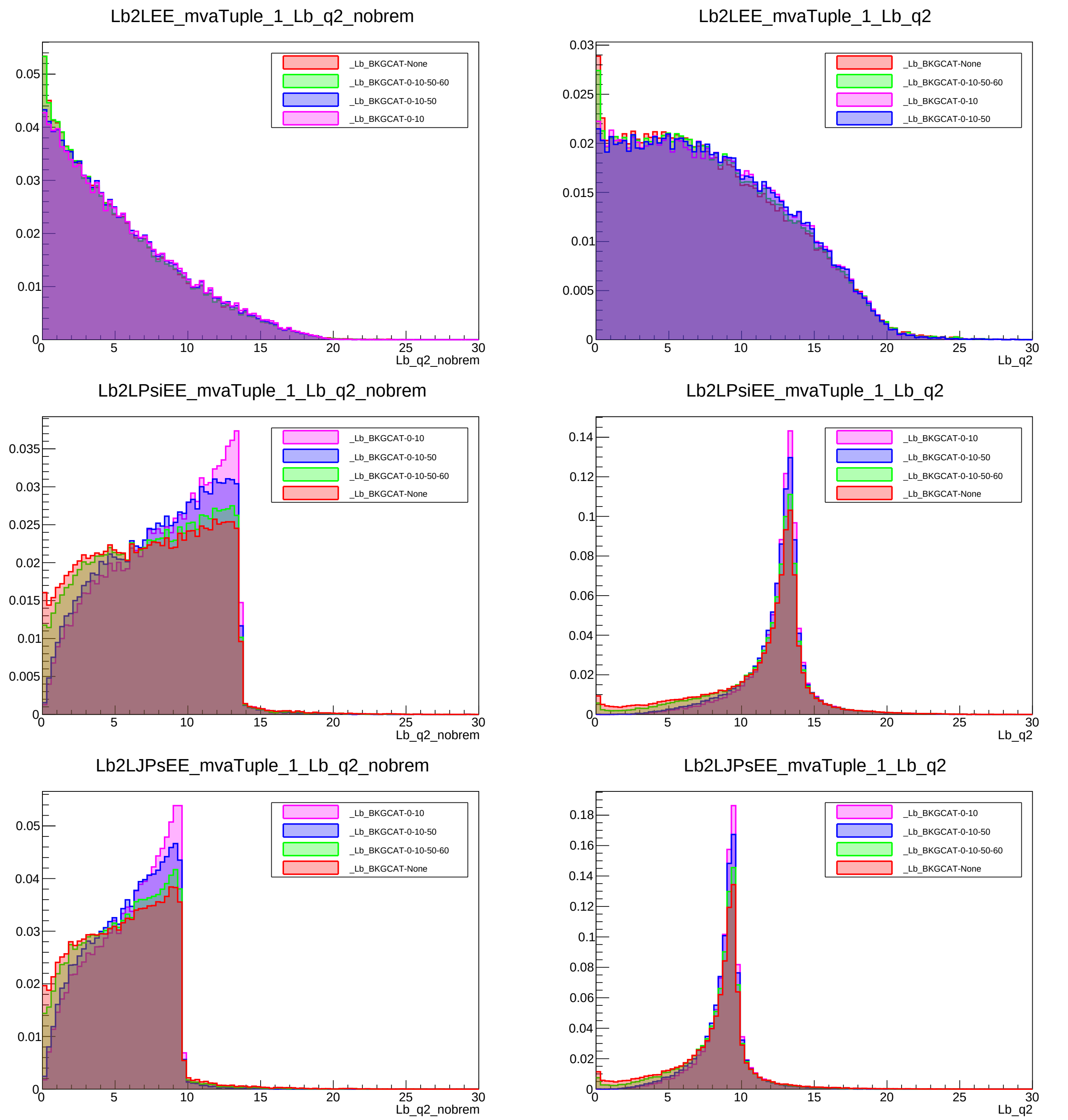

Figure 13. Variations in event distributions over `Lb_q2` (left) and `Lb_q2_nobrem` (right), for `Lb2LEE` (top), `Lb2LPsiEE` (middle) and `Lb2LJPsEE` (bottom) with background categories. Background categories considered are (None), (0 or 10), (0 or 10 or 50) and (0 or 10 or 50 or 60). Mass units are in GeV^2/c^4.

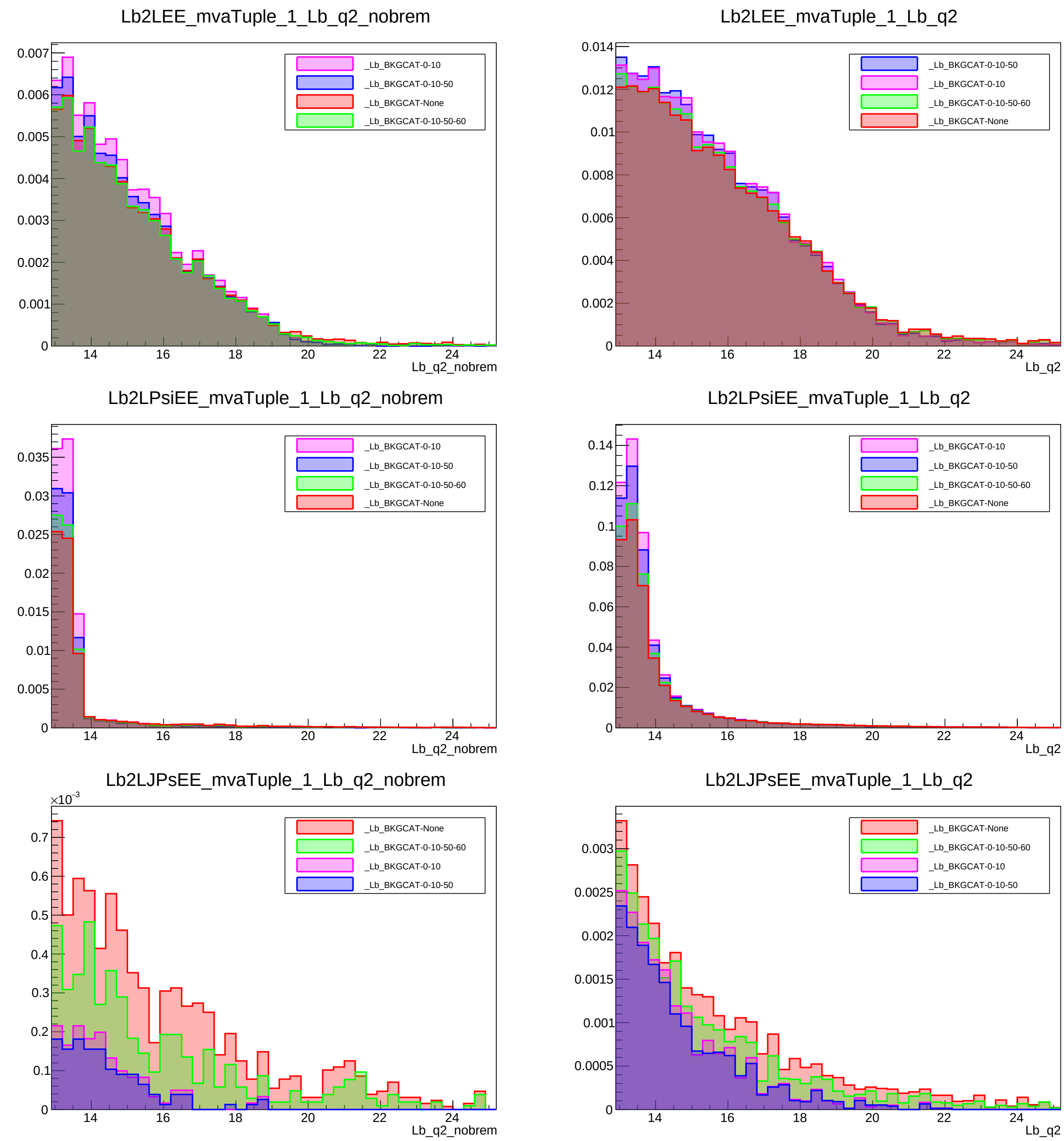

Figure 14. Variations in event distributions over `Lb_q2` (left) and `Lb_q2_nobrem` (right) range of interest, for `Lb2LEE` (top), `Lb2LPsiEE` (middle) and `Lb2LJPsEE` (bottom) with background categories. Background categories considered are (None), (0 or 10), (0 or 10 or 50) and (0 or 10 or 50 or 60). Mass units are in GeV$^2/c^4$.

A visually efficient way of checking on the `Lb2LPsiEE` and `Lb2LJPsEE` backgrounds is plotting their corresponding `Lb_q2` and `Lb_q2_nobrem` variables against each other, as shown in Figure 15. On the title of each of its graphs, it is mentioned the type of background categories that have been applied. It is possible to see two areas of clearance when the types of event are constrained to just signal and quasi-signal (bottom-right graph). The first area is at high $q^2 \in (13, 25)$ and the second is at low $q^2 \in (3, 3)$ (more or less). Those two areas have been zoomed-in in Figures 17 and 16. The almost inexistence of the charmonium backgrounds in Figure 16 is expected due to proximity of the photon pole, and it is also consistent with experimental observations at LHCb [27].

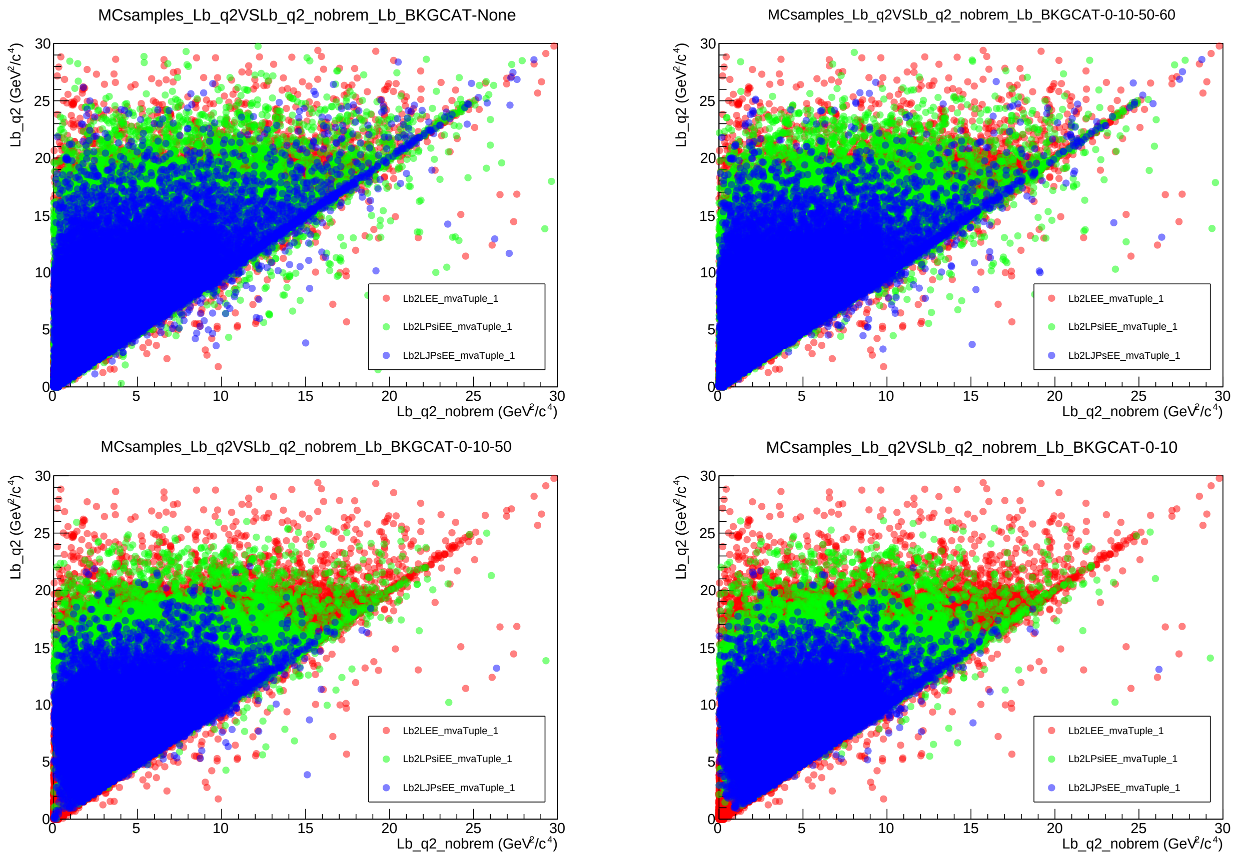

Figure 15. Plot of `Lb_q2` against `Lb_q2_nobrem`. Background conditions vary between graphs and are specified in the title. Red color indicates the signal, `Lb2LEE`, blue color indicates background from `Lb2LPsiEE`, and green indicates background from `Lb2LJPsEE`. Mass units are in GeV^2/c^4.

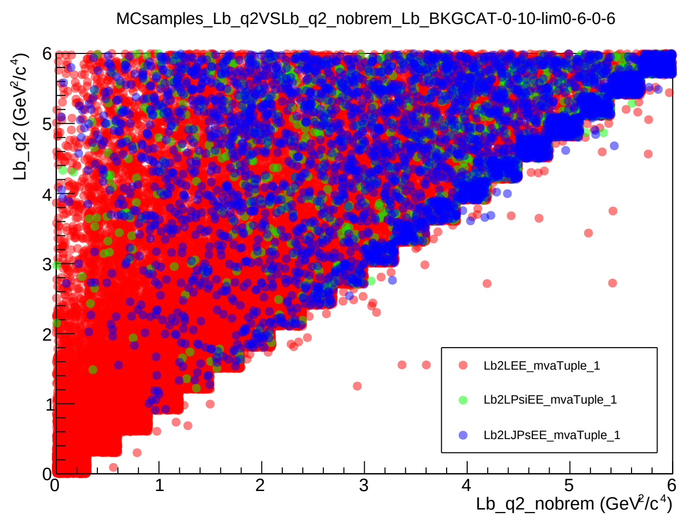

Figure 16. Plot of `Lb_q2` against `Lb_q2_nobrem` in the range $q^2 \in [0.6]$ GeV^2/c^4. Background conditions are `Lb_BKGCAT == 0 || Lb_BKGCAT == 10`, for both signal and backgrounds.

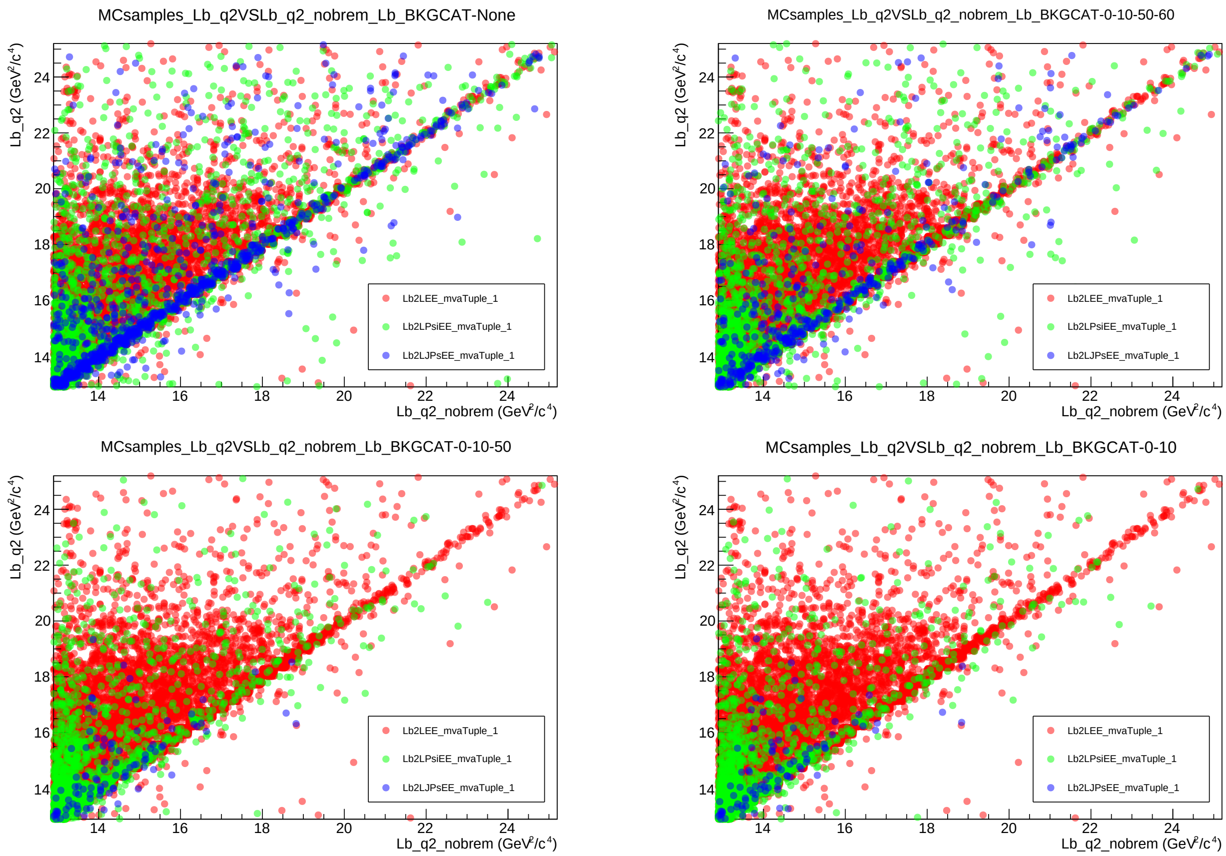

Figure 17. Plot of `Lb_q2` against `Lb_q2_nobrem` in the range [13,25] GeV^2/c^4. Background conditions vary between graphs and are specified in the title. Red color indicates the signal, `Lb2LEE`, blue color indicates background from `Lb2LPsiEE`, and green indicates background from `Lb2LJPsEE`.

These comparisons show that any cut-definition on q^2 or q^2_{nobrem} aimed at separating background from signal events is going to be challenging.

6. Studies on backgrounds with RapidSim

Monte Carlo samples constitute a very robust way of studying the kinematic properties of the signal decay of interest as well as the potential backgrounds that can be introduced via other particle decays that have been imperfectly reconstructed in the detector. However, it typically takes a long time to generate these background samples, and a fair amount of memory to store them.

RapidSim is an application (which one can easily clone from their Github repository [28] into their local computer) that allows analysts to quickly generate these samples (in a matter of a few seconds, one is able to compute a million of events) with results approximate what can be obtained from a full detector simulation.

In our case, the speed of generation allows us to quickly perform initial studies that may indicate avenues for further investigation that may require more detailed simulations which are worth the time and memory expenditure.

My work with RapidSim faced two fronts: first, determine what type of Bremsstrahlung reconstruction is being applied during simulation; and, second, once this is known, compute potential background decays.

6.1. How does RapidSim work

There are two inputs for RapidSim simulations: the `.decay` file (which would correspond to the descriptor file in the Monte-Carlo Simulations), and a `.config` file. Consider the decay $\Lambda_b \to \Lambda(\to p^+\pi^-)e^+e^-$, which is assigned the following name in a simulation: `Lb0_L0_PPiEE`. When reading `Lb0_L0_PPiEE.decay` one sees:

```
$ cat Lb0_L0_PPiEE.decay
Lambdab0 -> { Lambda0 -> p+ pi- } e+ e-
```

And the `Lb0_L0_PPiEE.config` file looks as follows:

```
$ cat Lb0_L0_PPiEE.config
geometry : LHCb
paramsDecaying : M, P, PT
paramsStable : P, PT
paramsTwoBody : M2
param : M_PPiEE M 2 3 4 5
param : M_PPiEE_TRUE M 2 3 4 5 TRUE
param : M2_EE_TRUE M2 2 3 TRUE
param : M2_EE M2 2 3
cut : M_PPiEE min 4.9
cut : M_PPiEE_TRUE min 4.9
@0
  name : Lambdab0_0
@1
  name : Lambda0_0
@2
  name : ep_0
  smear : LHCbElectron
@3
  name : em_0
  smear : LHCbElectron
@4
  name : pp_0
  smear : LHCbGeneric
@5
  name : pim_0
  smear : LHCbGeneric
```

To run RapidSim one simply needs to set-up the OS environment as specified in the repository and provide a decay file. RapidSim will automatically generate a configuration file that can be later modified for subsequent runs.

Each line in `Lb0_L0_PPiEE.config` follows the structure `<setting : value>`. The line

`param : M_PPiEE M 2 3 4 5`

for instance is user-defined. It can be read as follows: 'Define a parameter called `M_PPiEE` which stores the `M` (mass) value of the system comprised of the particles with ID numbers 2, 3, 4 and 5'. When we look down the file we see that the particle with ID $= 2$ corresponds to `ep_0` ('electron plus'), the positron; that the particle with ID $= 3$ corresponds to `em_0` ('electron minus'), the electron; that the particle with ID $= 4$ corresponds to `pp_0` ('proton plus'), simply the proton; and that the particle with ID $= 5$ corresponds to `pim_0` or 'pion minus'. Each of those particles has also been assigned a `smear` function, which is either `LHCbGeneric` or `LHCbElectron`.

Another added line is that which concerns a `cut`. For instance,

`cut : M_PPiEE min 4.9`

sets a limit on the minimum value for the pre-defined variable `M_PPiEE` of 4.9 GeV/c^2. Setting limits such as this, allow to reduce the space from which events are generated in the simulation, and hence increase the resolution in regions of interest.

6.2. RapidSim and Bremsstrahlung radiation

At the moment, the RapidSim repository does not explicitly offer an option to investigate the variation in event distributions for `Lb_q2` and `Lb_q2_nobrem` with Bremsstrahlung photon multiplicity. In fact, our initial question was: which multiplicity is being applied to the electron-positron pair when the smearing function is set to the default `LHCbElectron` in the `.config` file?

With that question in mind, results from a RapidSim run using 10^6 data points and `<smear : LHCbElectron>` were compared to those from the MC samples, for the $\Lambda_b \to \Lambda e^+ e^-$ decay (Figure 18). The conclusion drawn from these graphs is that `LHCbElectron` is an smearing function which approximates the electron momenta distribution assuming no Brem multiplicity. Another thing to note is that, unlike the MC simulation, RapidSim does not include the resonance for the direct photon production $b \to s\gamma$ (the photon pole at low q^2).

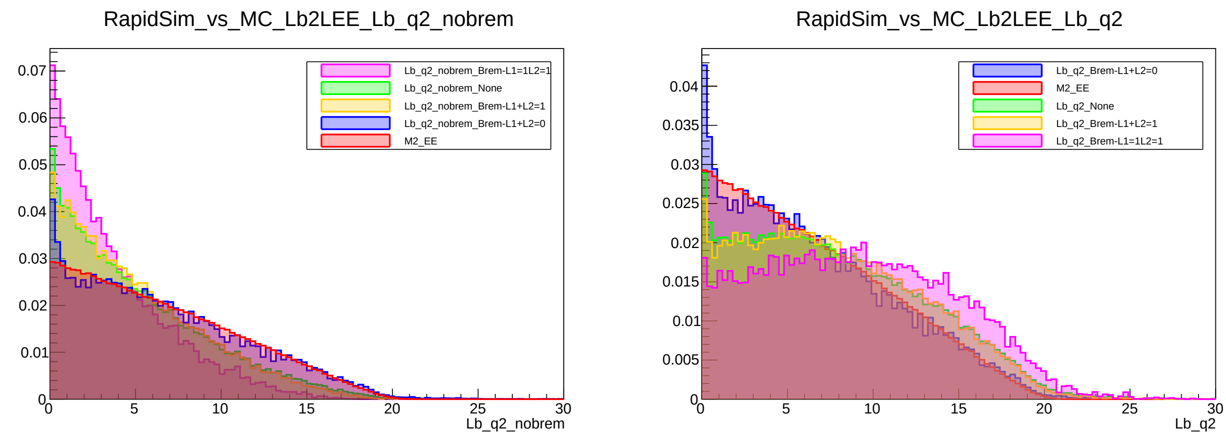

Figure 18. Comparison of the distributions of the squared invariant mass of the dielectron system from RapidSim and from a full Monte Carlo simulation with different multiplicities (difference in color). At the left, `M2_EE` from RS is compared to `Lb_q2_nobrem` from MC, and at the right `M2_EE` from RS is compared to `Lb_q2` from MC.

The second question after this was: what can we do to be able to consider other smearing functions in the RapidSim simulations? I started looking more thoroughly around the Github repository and found an old commit for `config/smear/LHCbElectron`, shown in Figure 19.

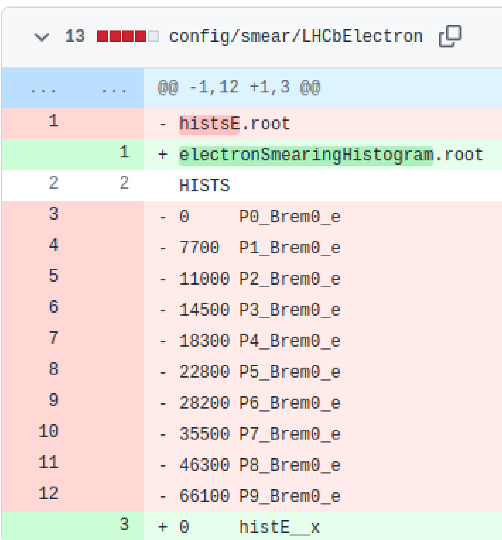

Figure 19. Most recent changes in the `LHCbElectron` on the RapidSim Github repository.

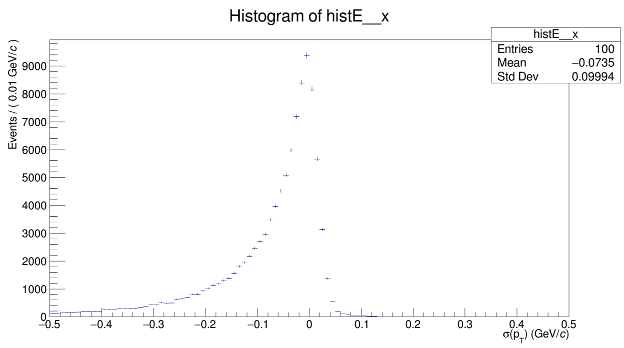

Figure 20. Distribution of `histE__x` histogram, provided in the `electronSmearingHistogram.root` file specifies in `LHCbElectron`.

The file `LHCbElectron` is an ASCII file which is input in the `.config` file of a decay as an smearing function for electrons (see the example above). It contains two pieces of information: the `root` file, which holds the momentum distribution we wish to consider in our simulation; and a table, arranged in two columns, with the first one specifying the lower edge of a p bin, and the second specifying the name of the `TH1` object describing the resolution function in that bin [29]. Currently, it looks like this

```
$ cat LHCbElectron
electronSmearingHistogram.root
HISTS
0 histE__x
```

If one checks the `electronSmearingHistogram.root` file, one finds:

```
root [0] TFile* f = new TFile("
    electronSmearingHistogram.root")
(TFile *) 0x262fbb0
root [1] f->ls()
TFile**         electronSmearingHistogram.
    root
 TFile*         electronSmearingHistogram.
    root
  KEY: TH1F      histE__x;1   Histogram of
     histE__x
```

A quick plot of `histE__x` is shown in Figure 20. It does not only resemble a crystal-ball function, but indeed it is crystal-ball, as can be deduced from the `RooCBShape` function found at `utils/generateElectronSmearingHistogram.C`.

Coming back to Figure 19, the `LHCbElectron` file used to call the `histsE.root` instead, which contains the following:

```
root [0] TFile* f = new TFile("histsE.
    root")
(TFile *) 0x2bb5c60
root [1] f->ls()
 TFile**    histsE.root
  TFile*    histsE.root
   KEY: TH1F  P0_Brem0_e;1
   KEY: TH1F  P0_Brem1_e;1
   KEY: TH1F  P0_Brem2_e;1
   KEY: TH1F  P1_Brem0_e;1
   KEY: TH1F  P1_Brem1_e;1
   KEY: TH1F  P1_Brem2_e;1
```

The name of the histograms in this file follows the format `PX_BremY_e`, wherre `X` rusn from 0 to 9 and `Y` runs from 0 to 2.

Could this be what we were looking for? Figure 21 shows the too-many-times-seen-already crystal-ball shape. It is antisymmetric about $\sigma(p_\perp) = 0$. This makes sense, as for `Brem0` it is assumed that the electron arrived along with the radiated Bremsstrahlung photon, and therefore no recovery is needed. In that case the electron's reconstructed momentum will always be equal or lower than it truly was during the decay.

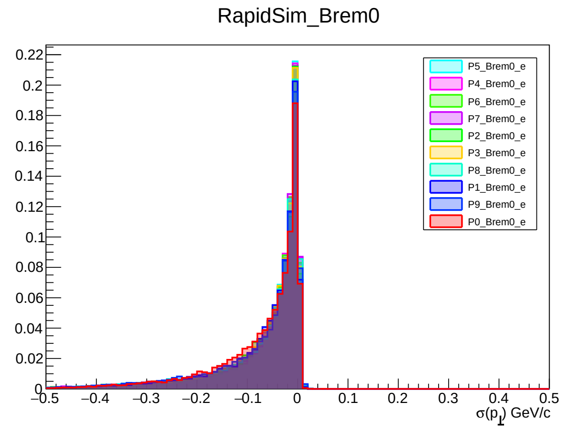

Figure 21. Histograms for `Brem0` from the `histsE.root` file in RapidSim. Different colors correspond to different momentum bins.

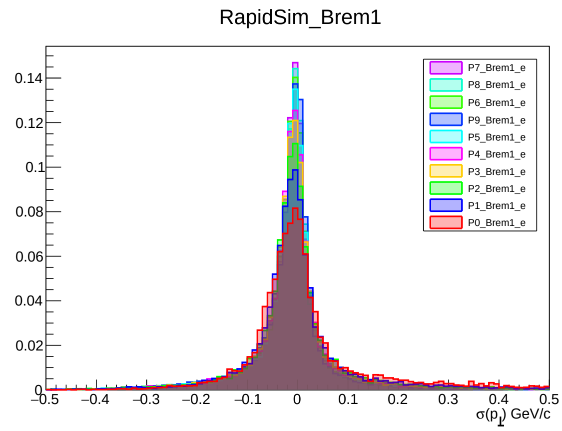

Figure 22. Histograms for `Brem1` from the `histsE.root` file in RapidSim. Different colors correspond to different momentum bins.

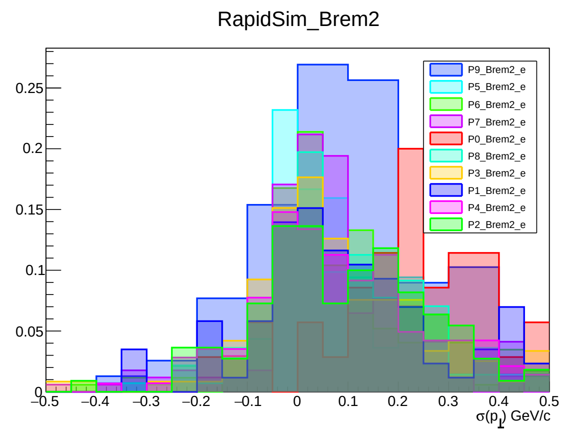

Figure 23. Histograms for `Brem2` from the `histsE.root` file in RapidSim. Different colors correspond to different momentum bins.

Figure 22 shows an almost symmetric distribution about $\sigma(p_\perp) = 0$. This also makes sense, as for `Brem1`, the electron is assumed to have radiated a Bremsstrahlung photon upstream in the detector. Sometimes it will have actually radiated a photon and sometimes not; therefore recovering the radiated photon's momenta will shift that of the electron to sometimes higher, and sometimes lower values, respectively.

Figure 23 shows a noisier distribution, but a similar reasoning can be applied, and the electron's momentum will more likely be overestimated than underestimated.

In conclusion, we seemed to have found a way of accounting for Bremsstrahlung radiation in our simulations in RapidSim. Everything that was needed to do was to create three additional ASCII files (call them `LHCbElectron_Brem0`, `LHCbElectron_Brem1` and `LHCbElectron_Brem2`) and in each of them, following the previous format shown in red in Figure 19, add the references to `histsE.root` and the `PX_BremY_e` histograms appropriate to the `Brem`[10].

Then, `LHCbElectron_BremY` (with `Y` = 0, 1, 2) is effectively a smearing function that can be applied to the individual electron such that

- `LHCbElectron_Brem0` assigns no photon-multiplicity;
- `LHCbElectron_Brem1` assigns a photon-multiplicity of 1; and
- `LHCbElectron_Brem2` assigns a photon-multiplicity of 2.

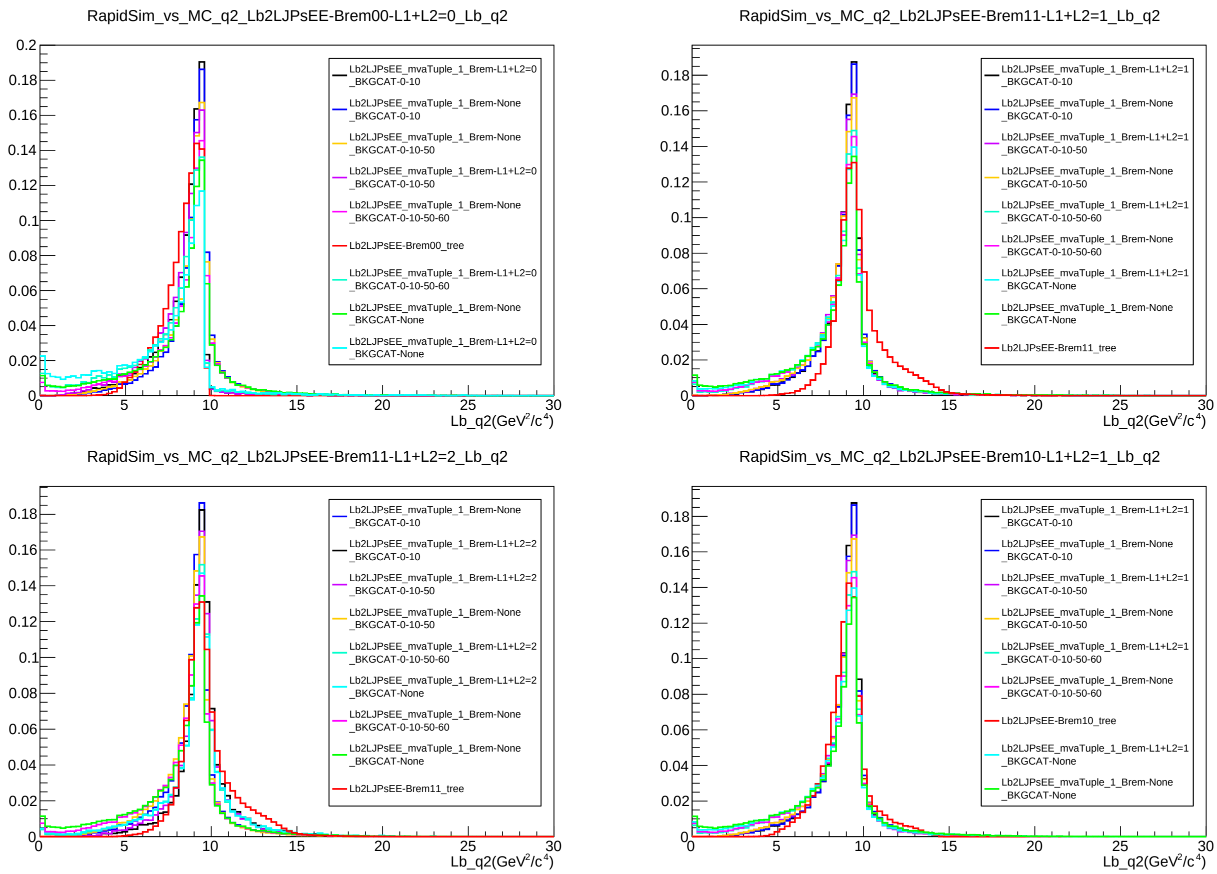

Figure 24. Distribution of `M2_EE` (red) against other `Lb_q2` distributions (rest of colors) from the MC sample for the same decay. The MC distributions are subjected to different background conditions, which can be found in the legend. Each graph compares the outputs from the two different simulations with different or what should be equal Bremsstrahlung conditions.

[10] The same binning numbers from Figure 19 were applied in all `LHCbElectron_BremX` files.

To test the performance of RapidSim simulations, the distributions for `M2_EE` for different smearing functions were compared to those for `Lb_q2` from a full Monte-Carlo simulation for the decay `Lb2LJPsEE`. The comparisons included the application of different background and photon-multiplicity conditions on the MC. These comparisons are found in Figure 24. Out of the four graphs one is expected to be off-pitch. This is the the top-right plot, which compares a RS run with both electrons with `LHCbElectron_Brem1` against a MC run which considers only one of the electrons to have a one photon-multiplicity. Considering that the average timing for a RapidSim simulation is of 30 seconds, the matchings in the other three graphs is impressive. Zooming-in at the bottom-right graph is possible to see that the closest fittings to the red distribution are the blue/black colors, which correspond to the 'pure' `Lb2LPsEE` signal with and without photon-multiplicity conditions applied. This makes sense as for what the `Lb_q2` variable is concerned, as double the amount of events will consist of one photon assigned for the two-electron system compared to other cases.

Finally, Figure 25 shows four different 2D plots obtained from simulations in RapidSim of the $\Lambda_b \to \Lambda(\to p^+\ \pi-)e^+\ e^-$ decay. In each, the invariant mass squared of the dilepton system is put against the invariant mass of the final-state particles of the decay. As one may expect, the larger the number of photon recoveries assigned to the electrons, the more the event distribution expands over high q^2 and high $m[p\pi^- e^+ e^-]$ values.

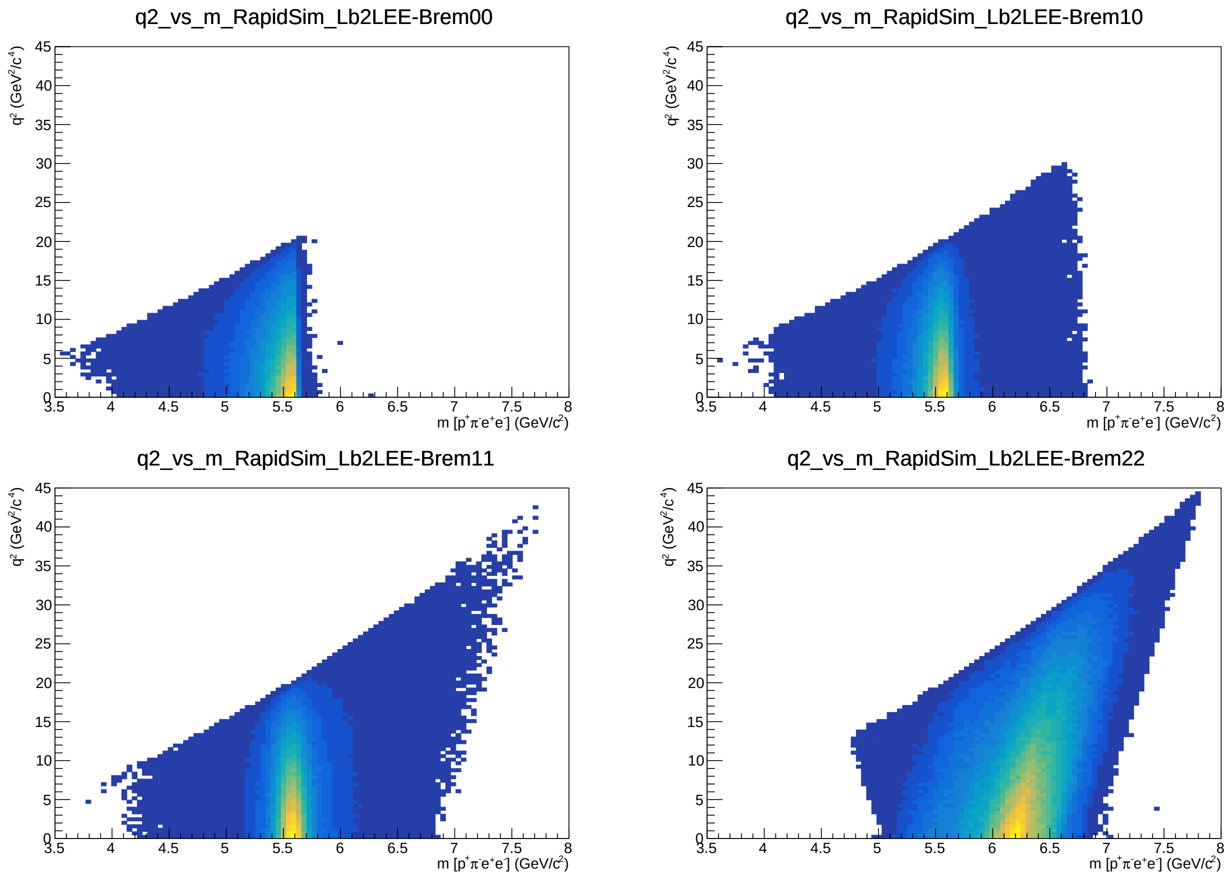

Figure 25. Each graph plots the square of the dilepton invariant mass against the invariant mass of the final-state particles of the signal decay. The two integers following 'Brem' in the title (e.g., Brem00) refer to the photon multiplicities applied to each electron.

I have gathered in Figure 26 similar graphs to those from Figure 25 but using the data from a full Monte Carlo simulation. While all events in the plots in Figure 25 have been generated applyin a specific Bremsstrahlung recovery, when applying photon-multiplicity conditions on the MC samples we are just selecting the events which fulfilled those conditions, not generating them from them. Therefore the plot corresponding to `L1_BremMultiplicity == 2  L2_BremMultiplicity == 2` in MC, which translates to `Brem22` in RS, is almost empty, as it is highly unlikely that the two electrons will be assigned two photon reconstructions. In fact, the drastic drop in the amount of events in the transition from `Brem-L1=1L2=1` to `Brem-L1=2L2=1` indicates the low probability of having two photons assigned for the momentum reconstruction of an electron.

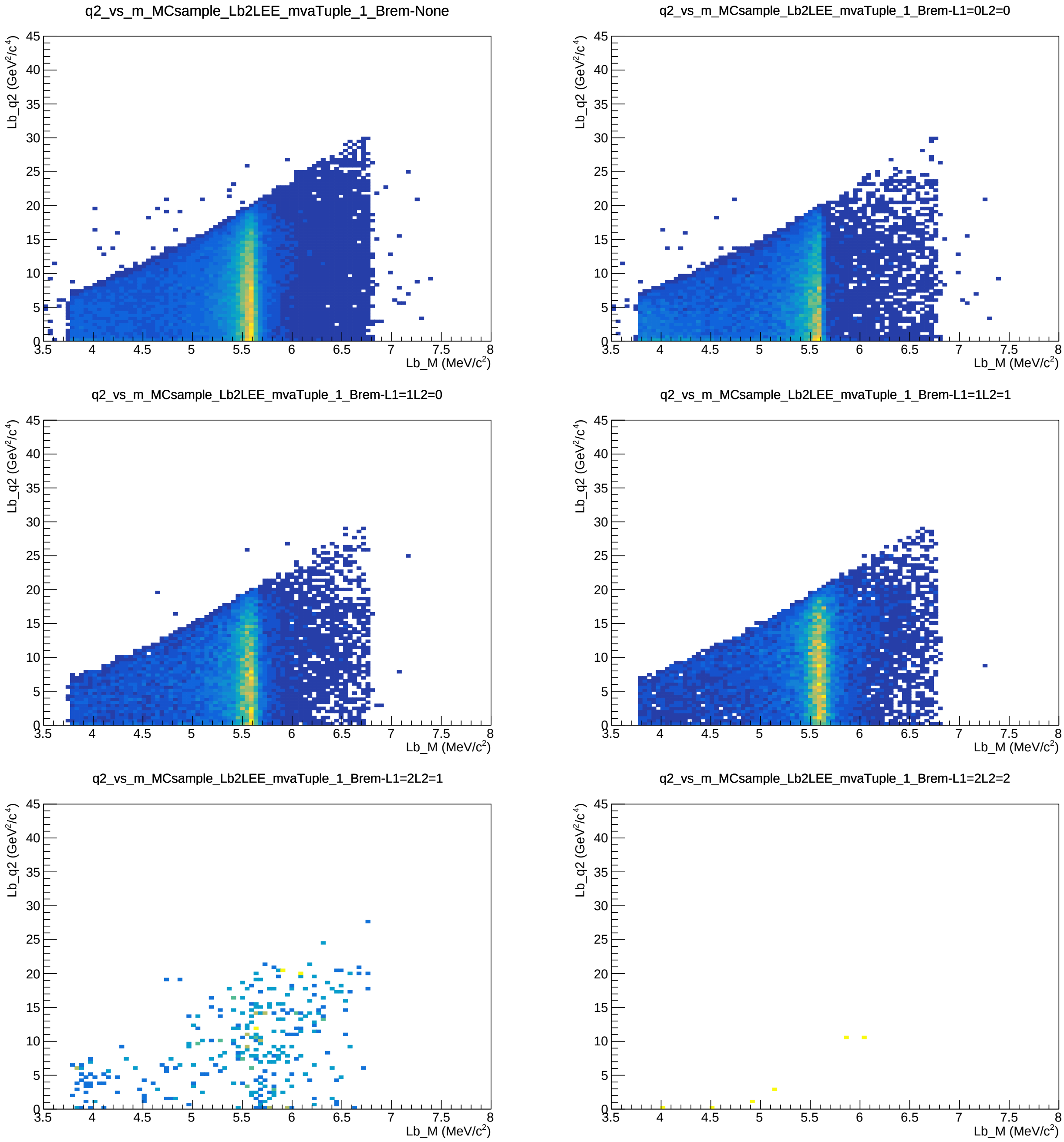

Figure 26. Each graph plots the square of the dilepton invariant mass against the invariant mass of the final-state particles of the signal decay. The photon-multiplicity condition that is applied on each is written at the end of the title (e.g., 'Brem-L1=1L2=2' means a condition: `L1_BremMultiplicity == 1  L2_BremMultiplicity == 2`.

6.3. RapidSim and partially-reconstructed backgrounds

As has been explained, partially-reconstructed backgrounds can arise when a subset of all the final-state particles corresponding to a certain decay is used for reconstruction, and this same subset corresponds to the full set of the final-state particles of the signal decay. Therefore, the first (partially-reconstructed) decay may be categorised as a signal decay. The $\Lambda_b \to \Lambda(\to p^+ \pi^-)e^+ e^-$ decay is exposed to quite a few background events of this type. In what follows, therefore, I will simply consider some of them.

Excited-Λ baryons

Decays involving excited Lambdas ($\Lambda(1405), \Lambda(1520), \Lambda(1600)$ in this paper) have been simulated according to the following decay chain:

$$\begin{aligned} \Lambda_b^0 &\to \Lambda^* \; e^- \; e \\ &\quad \Lambda^* \to \Sigma^0 \pi^0 \\ &\qquad\quad \Sigma^0 \to p^+ \; \pi^-, \end{aligned}$$

where Λ^* refers to the Λ-baryon in the excited state. Computing the invariant mass $m[p\pi^- e^+ e^-]$, one would obtain a signal candidate by ignoring the π^0 meson in the reconstruction.

The two Ξ_b^0 and Ξ_b^- baryons

Decays involving the two Ξ_b^0 and Ξ_b^- baryons have been simulated according to the following decay chain:

$$\begin{aligned} \Xi_b^0 &\to \Xi^0 \; e^- \; e \\ &\quad \Xi^0 \to \Lambda^0 \pi^0 \\ &\qquad\quad \Lambda^0 \to p^+ \; \pi^-, \end{aligned} \qquad \text{and} \qquad \begin{aligned} \Xi_b^- &\to \Xi^- \; e^- \; e \\ &\quad \Xi^- \to \Lambda^0 \pi^- \\ &\qquad\quad \Lambda^0 \to p^+ \; \pi^-, \end{aligned}$$

respectively. Computing the invariant mass $m[p\pi^- e^+ e^-]$ for these decays ignores the π^0 and π^- in each case.

The Ω_b^- baryon

The decay concerning the Ω_b^- baryon has been simulated according to the following decay chain:

$$\begin{aligned} \Omega_b^- &\to \Omega^- \; e^+ \; e^- \\ &\quad \Omega^- \to \Lambda^0 \; K^- \\ &\qquad\quad \Lambda^0 \to p^+ \; \pi^-, \end{aligned}$$

Computing the invariant mass $m[p\pi^- e^+ e^-]$ for this decay ignores the K^- meson.

In Figure 27, the invariant mass of our signal has been plotted using the data from the MC sample, as well as from a RapidSim simulation[11]. It is compared to the invariant mass distributions obtained from the partially-reconstructed backgrounds described above and computed in RapidSim. The violet and black colors correspond to the Ξ_b and Ξ_b^0 decays respectively; the green, yellow and dark-blue colors are associated to the Λ excited-state decays (the wider, the heavier, the greater the number), and the histogram in cyan corresponds to the distribution from the Ω^- decay. The performance of the software in approximating the full Monte-Carlo simulation is, again, remarkable. It also builds a greater confidence on the trustfulness of the other distributions.

More interesting perhaps, is Figure 28, which shows the same invariant mass distributions but to which a $q^2 > 13$ GeV$^c/c^4$ condition (high q^2 region!) has been applied. The partially-reconstructed backgrounds from the two Ξ baryons overlap with the signal quite significantly.

[11] I hope you can zoom in!

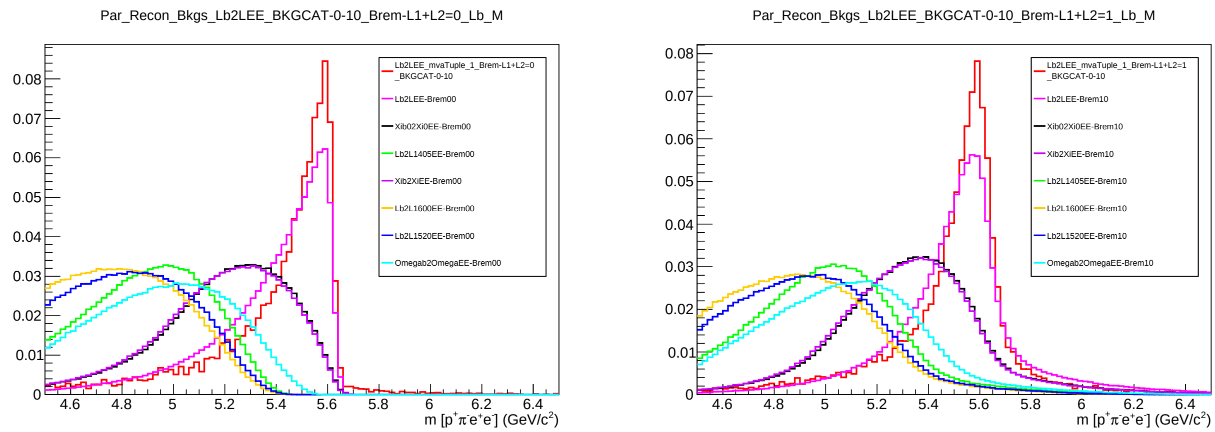

Figure 27. Normalised distributions of the $m[p\ \pi^- e^+\ e^-]$ invariant mass for the MC signal decay (red), the RapidSim signal decay (magenta) and various partially-reconstructed backgrounds computed also in RapidSim (rest). Their different topologies have been described in the main text. At the left, a Brem00 condition has been applied in all simulations; at the right, a Brem10 condition has been considered instead.

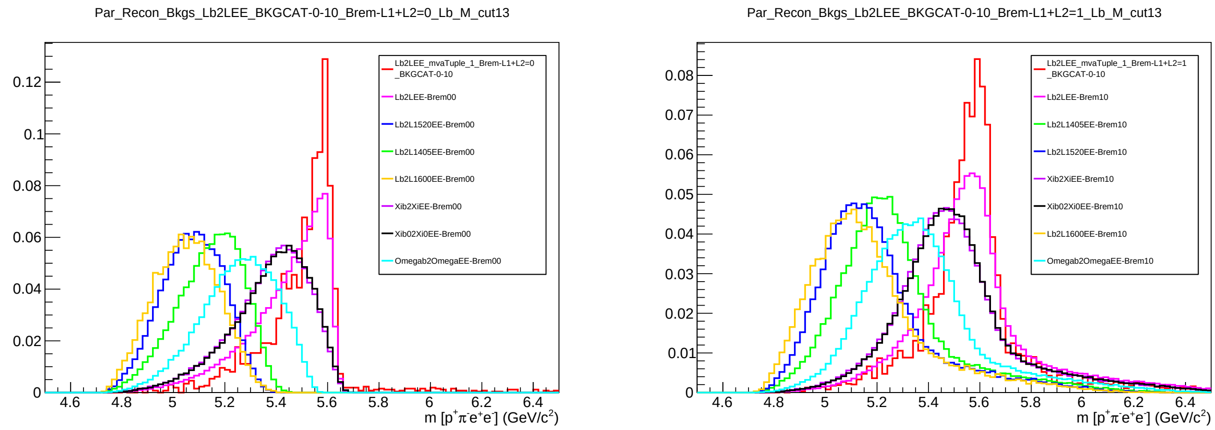

Figure 28. Normalised distributions of the $m[p\ \pi^- e^+\ e^-]$ invariant mass for the MC signal decay (red), the RapidSim signal decay (magenta) and various partially-reconstructed backgrounds computed also in RapidSim (rest). Their different topologies have been described in the main text. At the left, a Brem00 condition has been applied in all simulations; at the right, a Brem10 condition has been considered instead. In all of them, were subjected to constriction on the value of q^2 such that $q^2 > 13\ \mathrm{GeV}^2/c^4$.

7. Discussion, suggestions, comments

A few comments on this research, suggestions on improvements and further investigations will be made in the following.

Defining `Lb_q2_nobrem` and `Lb_q2_nobrem` cuts to train a BDT.

Advances on the $\Lambda_b \to \Lambda l^+ l^-$ analysis will require the usage of machine-learning algorithms (i.e., boosted-decision trees) to discern between signal and background events in the real data. This knowledge must be acquainted from information provided by scientists on what can be and cannot be considered signal. The study performed on this paper on the overlapping of the two resonant decays `Lb2LPsiEE` and `Lb2LJPsEE`, with the `Lb2LEE` decay of interest through the full MC samples, points to a future challenge in determining a cut between signal and background. This separation at high q^2 will be difficult, but not necessarily unfeasible. A good understanding of the strengths and flaws of RapidSim might help with the issue.

Studies of Bremsstrahlung radiation with RapidSim.

A very careful analysis of the backgrounds will be needed. These would ideally be studied through

Monte Carlo computations that simulate the full experiment in a meticulous manner. With the inconvenience of the limited time and memory resources, RapidSim is able to provide a quick estimate for the effects of partially-reconstructed backgrounds due to Bremsstrahlung radiation.

However, currently, the only properly available momentum-smearing function in RapidSim for electrons is that which assigns zero photon multiplicity. It was found in an old Github commit message in the RapidSim repository that distributions which consider one and two Bremsstrahlung recoveries used to be available. After the 'update to use LHCb electron smearing based on e mu analysis', the possibility of considering these disappeared. It would be for the interests of both the developers and users that wish to perform quick checks on potential partially-reconstructed backgrounds to make them explicitly accessible (i.e., by creating another two separate `LHCbElectron_Brem1` and `LHCbElectron_Brem2` files, as was done for the study discussed in this paper).

Studies of other partially-reconstructed backgrounds.

Unlike a MC sample, RapidSim does not offer the possibility to extract events which fulfill certain background-category conditions. However, it can be used for other types of studies, such as the ones described in this report. By modifying the `.config` file as desired, it is possible to tell RapidSim to compute the invariant mass of a decay which, due to partial reconstruction, happens to match the signal, as have been shown in the previous section. This, hence, constitutes another area in which the software could be helpful.

Acknowledgements

I will be honest and write in here (especially because I expect very few people to ever actually read this), that CERN has become for me, *the* Wonder of the Modern World. It is a piece of art that cannot be described in an audio-guide in a museum - it does not fit in one anyways-. Its beauty, more than on the physical wires and magnets that are used in its facilities, resides on how they are all set-up and connected to build such a magnificent device as any of its instruments is. And that brings the arousal of beauty, when things are easy but not simple. I have, through this internship, discovered that a lot of CERN's charm resides not only on its large installations, but from its fractal structure in its workings. Behind a reported measurement and its uncertainty, there is the time and the thoughts of thousands of people, each one doing a small 'easy' thing, that adds to many others in such a way as to bring discoveries like the Higgs - which is not a simple task at all!-. The phrase that comes to mind is that of *divide et impera*. All big projects in the history of humanity are founded on these three words. Here it is thus, my grain of sand.

I was granted, and I, honoured, accepted, the possibility to work in the research endeavours of LHCb this year. I did enjoy all of what this experience has involved. The extensive lecture program and organised virtual tours around the facilities at CERN, have managed to increase even more my curiosity in particle physics. I found them a pleasure to attend to because of the passion of all of the lecturers and staff involved. I have also met an incredible group of students which, I hope, I will keep contact with for a long while. I can be no less than very grateful to the organisers of the CERN Summer Student Program for making that possible.

I would also like to thank the Lb2Lll group for always being willing to help when I needed it, and for bearing with me during the entire summer; with my weekly and sometimes very messy presentations, and with my questions and sometimes very silly mistakes. Especially, however, I would like to thank my supervisor, Mick Mulder, for his constant support and patience during the internship, for never putting a boundary to my curiosity, and for the very constructive feedback he provided for this report (particularly when he did it over the weekend!).

References

[1] LHCb Large Hadron Collider beauty experiment CERN. *3 June 2014: An interesting result presented at the LHCP conference.* URL: https://lhcb-public.web.cern.ch/.

[2] Sebastien Descotes-Genon et al. "Implications from clean observables for the binned analysis of $B- > K * \mu^+\mu^-$ at large recoil". In: *JHEP* 01 (2013), p. 048. DOI: 10.1007/JHEP01(2013)048. arXiv: 1207.2753 [hep-ph].

[3] CERN. *Intriguing new result from the LHCb experiment at CERN.* URL: https://home.cern/news/news/physics/intriguing-new-result-lhcb-experiment-cern.

[4] BBC. *Machine finds tantalising hints of new physics.* URL: https://www.bbc.co.uk/news/science-environment-56491033.

[5] Ian Sample Science editor for The Guardian. *Cern experiment hints at new force of nature.* URL: https://www.theguardian.com/science/2021/mar/23/large-hadron-collider-scientists-particle-physics.

[6] Roel Aaij et al. *Test of lepton universality in beauty-quark decays.* Tech. rep. All figures and tables, along with any supplementary material and additional information, are available at https://cern.ch/lhcbproject/Publications/p/LHCb-PAPER-2021-004.html (LHCb public pages). Geneva: CERN, 2021. arXiv: 2103.11769. URL: https://cds.cern.ch/record/2758740.

[7] Patrick Koppenburg. *Flavour Anomalies.* URL: https://www.nikhef.nl/~pkoppenb/anomalies.html.

[8] IUPAC. Compendium of Chemical Terminology, 2nd ed. (the "Gold Book"). Compiled by A. D. McNaught and A. Wilkinson. Blackwell Scientific Publications, Oxford (1997). Online version (2019-) created by S. J. Chalk. ISBN 0-9678550-9-8. https://doi.org/10.1351/goldbook.

[9] Gerhard Buchalla, Andrzej J. Buras, and Markus E. Lautenbacher. "Weak decays beyond leading logarithms". In: *Rev. Mod. Phys.* 68 (4 1996), pp. 1125–1244. DOI: 10.1103/RevModPhys.68.1125. URL: https://link.aps.org/doi/10.1103/RevModPhys.68.1125.

[10] Marcel Materok. "Angular analyses and branching fraction measurements of b-hadron FCNC decays". In: (2021). URL: https://cds.cern.ch/record/2772332.

[11] The LHCb Collaboration et al. "The LHCb Detector at the LHC". In: 3.08 (2008), S08005–S08005. DOI: 10.1088/1748-0221/3/08/s08005. URL: https://doi.org/10.1088/1748-0221/3/08/s08005.

[12] CERN. *The Large Hadron Collider.* URL: https://home.cern/science/accelerators/large-hadron-collider.

[13] R. Aaij et al. "Measurement of B meson production cross-sections in proton-proton collisions at $\sqrt{s} = 7$ TeV". In: *Journal of High Energy Physics* 2013.8 (2013). ISSN: 1029-8479. DOI: 10.1007/jhep08(2013)117. URL: http://dx.doi.org/10.1007/JHEP08(2013)117.

[14] LHCb Large Hadron Collider Beauty Experiment. *The LHCb Detector, VErtex LOcator (VELO).* URL: http://lhcb-public.web.cern.ch/en/Detector/VELO-en.html.

[15] Marcin Kucharczyk, Piotr Morawski, and Mariusz Witek. *Primary Vertex Reconstruction at LHCb.* Tech. rep. Geneva: CERN, 2014. URL: https://cds.cern.ch/record/1756296.

[16] M Gersabeck. "LHCb Tracking, Alignment and Physics Performance". In: *PoS* VERTEX2010 (2010). LHCb-TALK-2010-052, 014. 11 p. URL: https://cds.cern.ch/record/1314528.

[17] G. Corti et al. "How the Monte Carlo production of a wide variety of different samples is centrally handled in the LHCb experiment". In: *Journal of Physics Conference Series.* Vol. 664. Journal of Physics Conference Series. Dec. 2015, 072014, p. 072014. DOI: 10.1088/1742-6596/664/7/072014.

[18] Vladimir Grigorov. *TupleToolMCBackgroundInfo < LHCb < TWiki.* URL: https://twiki.cern.ch/twiki/bin/view/LHCb/TupleToolMCBackgroundInfo.

[19] V. V. Gligorov. "Reconstruction of the Channel $B_d^0 \to D^+\pi^-$ and Background Classification at LHCb (revised)". In: (2007). URL: `https://cds.cern.ch/record/1035682/files/lhcb-2007-044.pdf`.

[20] The LHCb Collaboration, Ulrik Egede, and Tom Hadavizadeh. "Test of lepton universality with B0 $\to$ K*0+- decays". English. In: *Journal of High Energy Physics* 2017.8 (2017). ISSN: 1029-8479. DOI: `10.1007/JHEP08(2017)055`.

[21] Paula Alvarez Cartelle (LHCb). *Search for lepton flavour universality violation in $B^+ \to K^+l^+l^-$ decays*. URL: `https://indico.cern.ch/event/779306/attachments/1813851/2972219/LHCb_RK.pdf`.

[22] Mick Mulder. "The essence of rare beauty: Studying B0(s) $\to$ +- decays with the LHCb experiment". English. PhD thesis. University of Groningen, 2021. DOI: `10.33612/diss.149618058`.

[23] William Detmold and Stefan Meinel. "$\Lambda_b \to \Lambda l^+ l^-$ form factors, differential branching fraction, and angular observables from lattice QCD with relativistic b quarks". In: *Physical Review D* 93 (Apr. 2016). DOI: `10.1103/PhysRevD.93.074501`.

[24] R. Aaij et al. "Measurement of the differential branching fraction of the decay b0$\to$+-". In: *Physics Letters B* 725.1 (2013), pp. 25–35. ISSN: 0370-2693. DOI: `https://doi.org/10.1016/j.physletb.2013.06.060`. URL: `https://www.sciencedirect.com/science/article/pii/S0370269313005534`.

[25] Yu-Ming Wang, Yongfang Li, and Cai-Dian Lü. "Rare decays of Λb$\to\Lambda+\gamma$ and Λb$\to\Lambda$+l+l- in the light-cone sum rules". In: *The European Physical Journal C* 59 (2009), pp. 861–882.

[26] William Detmold and Stefan Meinel. " b $\to$ + - form factors, differential branching fraction, and angular observables from lattice QCD with relativistic b quarks". In: *Physical Review D* 93.7 (Apr. 2016). DOI: `10.1103/PhysRevD.93.074501`.

[27] R. Aaij et al. "Differential branching fraction and angular analysis of the decay B0$\to$K *0 + -". English. In: *Physical Review Letters* 108.18 (May 2012). ISSN: 0031-9007. DOI: `10.1103/PhysRevLett.108.181806`.

[28] D. C. Craik G. A. Cowan and M. D. Needham. *RapidSim*. URL: `https://github.com/gcowan/RapidSim`. (accessed: 30.09.2021).

[29] G. A. Cowan, D. C. Craik, and M. D. Needham. "RapidSim: An application for the fast simulation of heavy-quark hadron decays". In: *Computer Physics Communications* 214 (May 2017), pp. 239–246. DOI: `10.1016/j.cpc.2017.01.029`. arXiv: `1612.07489 [hep-ex]`.